Petrophysical and geochemical constraints on alteration processes in granites

Matěj Machek[a], Zuzana Roxerová[a], Vojtěch Janoušek[b], Martin Staněk[a], Eduard Petrovský[a], Miloš René[c]

[a] *Institute of Geophysics AS CR, v.v.i, Boční II/1401, 14131, Prague 4, Czech Republic, mates@ig.cas.cz*
[b] *Czech Geological Survey, Klárov 3, 118 21 Prague 1, Czech Republic*
[c] *Institute of Rock Structure and Mechanics AS CR, v.v.i, V Holešovičkách 41, 182 09 Prague 8, Czech Republic*

published in Studia Geophysica et Geodaetica 57 (2013) 710 – 740

The hydrothermal alteration of granites has large influence on their petrophysical properties. To reveal the impact of alteration on magnetic and porosity properties of granites we have conducted a complex study of effects of two largely independent alteration processes, related to chemically different fluids, in granites of the Vysoký Kámen stock (the Krudum granite body, Czech Republic). It includes the whole-rock geochemical, magnetic and pore-space characterization.

The alkali feldspathization resulted in decomposition of Li-mica, quartz removal, depletion in mafic cations and growth of new alkali feldspars (albite, K-feldspar), decreasing the overall magnetic susceptibility and disrupting the pore space by its discontinuation. The preservation of the orientation of the principal susceptibility axes is likely related with insignificant influence of the feldspathization process on the paramagnetic and diamagnetic phases orientation acquired during the magma emplacement.

The greisenization, on the other hand had considerably more significant effects on microstructure and physical properties of the granite. The microstructure was modified by the growth of large amounts of new phases (lithium mica, quartz and topaz). This changed the mineral density of the rock, the porosity, size and character of pores to larger, flatter and probably more connected. This led also to the complete reworking of the original AMS during the greisenization.

1 Introduction

The granites represent a widespread rock type in the crust and thus have been studied extensively in terms of their geochemistry, structure, and mineralization, (e.g. Paterson et al., 1989, 1998; Clarke, 1992; Pitcher, 1993; Clemens and Droop, 1998; Petford et al., 2000; Brown, 2001; Clemens, 2003; Chappell, 2004; Nabelek and Liu, 2004; Vigneresse, 2004; Bonin, 2008; Sawyer et al., 2011). The interpretation is often hindered by hydrothermal alteration, which is common at the last stages of granite evolution connected with cooling and degassing. The process of hydrothermal alteration has been studied mostly from the geochemical and mineralogical points of view mainly due to its economic potential (e.g. Beus, 1962; Scherba, 1970; Pollard, 1983; Cathelineau, 1986; Štemprok, 1987 Dolejš and Štemprok, 2001; Monecke et al., 2011). However, the hydrothermal alteration can also have large influence on petrophysical properties of the granite and only few works have been devoted to the petrophysical and related structural constrains (Štemprok et al., 1997; Rosener and Géraud 2007; Just and Kontny, 2012).

The metasomatic mineral changes of the granites during the hydrothermal alteration transform the rock microstructure, and thus have potentially large influence on magnetic and porosity characteristics of the rock (Štemprok, 1987; Štemprok et al., 1997; Dolejš and Štemprok, 2001). Such changes are of great significance for the structural/tectonic and rock massifs homogeneity studies. The structural studies in granites often rely on anisotropy of magnetic susceptibility (AMS) (Tarling and Hrouda, 1993; Bouchez, 1997; Borradaile and Jackson, 2010) and one of the key parameters for evaluation of the pluton's homogeneity are its porosity characteristics (e.g. IAEA, 2011).

The topaz-bearing granites of the Karlovy Vary–Eibenstock Pluton in western Bohemia (Czech Republic) associated with the significant concentrations of incompatible elements have been of economic interest but remain poorly-understood. The studied Vysoký Kámen stock is a part of the Horní Slavkov–Krásno Sn–W–Nb–Ta–Li ore district. These granites suffered greisenization and feldspathization leading to the development of inhomogeneous system. The alteration, and greisenization in particular, of topaz-bearing granites was connected with a strong influx of volatile-rich fluids and opening of the geochemical system for many geochemical species (Heinrich, 1990; Štemprok, 1987; Dolejš and Štemprok, 2001; Webster et al., 2004; Dolejš and Wagner, 2008).

In such a geological situation, we have an opportunity to detect the structural and porosity record of the alteration processes coupled with the geochemical context. This paper presents results of combined AMS, porosity and whole-rock geochemistry of alteration processes in the topaz-bearing Vysoký Kámen granite stock exploring extensive outcrops in the namesake active quarry and its surroundings.

2 Geological setting

The Karlovy Vary–Eibenstock Pluton forms a significant part of the Variscan Krušné Hory/Erzgebirge Batholith (Saxothuringian Zone, Bohemian Massif; Blecha and Štemprok 2012 and references therein). The Batholith belongs to one coherent and cogenetic, c. 400 km long plutonic megastructure of the Saxo-Danubian Granite Belt (Finger et al., 2009). Geochemically, five groups of granites may be distinguished in the Krušné Hory/Erzgebirge Batholith (Förster et al., 1998, 1999; Förster and Romer, 2010): (i) low-F biotite granites, (ii) low-F two-mica granites, (iii) high-F, high P2O5 Li-mica granites, (iv) high-F, low-P2O5 granites and (v) medium-F biotite granites.

The Vysoký Kámen stock forms a part of the Krudum granite body (KGB, c. 50 km2), a subsidiary intrusion of the Karlovy Vary–Eibenstock Pluton in Slavkovský les Mts. (Fig. 1), which shows a concentric structure (René, 1998; Breiter et al., 1999; Jarchovský, 2006). Its center is formed by porphyritic Třídomí (Mu–) Bt granite, surrounded to the NW by younger, topaz-bearing, two-mica Milíře granite. The youngest, topaz–albite

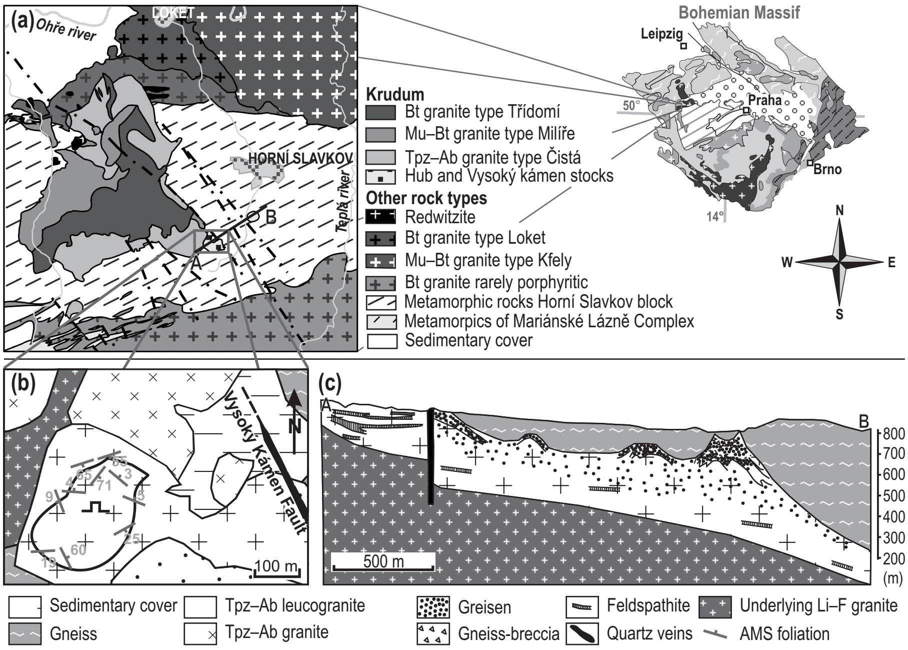

Fig. 1 *Simplified geological map showing: a) the position of the Vysoký Kámen stock within the Krudum granite body with vertical profile A–B marked. The smaller inset b) shows the Vysoký Kámen quarry with marked AMS foliation. c) Geological cross section of the Vysoký Kámen and Hub stocks after Jarchovský (2006).*

Čistá granite forms the outermost shell. The inner structure of the SE edge of the KGB, partly overlain by the Slavkov Crystalline Unit, is well stratified, comprising variably greisenized Čistá granites occurring also in the Hub and Schnöd granite stocks hosting a world-famous Sn–W mineralization of the Horní Slavkov–Krásno ore district. The granites of the KGB belong to medium-F biotite (Třídomí granite) and high-F, high P2O5 Li-mica (Milíře and Čistá granites) groups. The magmatic structure of the KGB is characterized by subhorizontal planar fabric which is locally replaced by the WNW–ESE and NE–SW trending fabrics, with predominant steep patterns in the most fractionated Čistá type (Machek et al., 2011).

The magmatic activity in the area of the Karlovy Vary–Eibenstock Pluton shows large time span between 325 ± 6 Ma and 290 ± 5 Ma for dioritic intrusions in the southern Nejdek–Eibenstock Massif and anorogenic rhyolite dykes respectively (Breiter et al., 1999; Kempe et al., 2004; Romer et al., 2007; Kovaříková et al., 2007, 2010).

The Vysoký Kámen stock in the SE part of the KGB is formed by topaz–albite leucogranite. Together with the alkali-feldspar syenite, it represents an apical parts of a highly fractionated granite body. It crystallized from residual magmas oversaturated with respect to alkalis and fluorine (René, 1998; Breiter et al., 1999; Jarchovský, 2006). Locally, irregular lenses and dykes of pegmatites oriented in NE–SW, NW–SE and NNW–SSE directions are present. These were probably co-magmatic with the leucogranites and developed from their granitic parental melts.

The main part of the Vysoký Kámen stock formed by the leucogranite and syenite lacks any manifestation of magmatic fabric in outcrop scale except rare subhorizontal magmatic layering of granites with unidirectional solidification textures (UST). The variously greisenized leucogranite occurs in form of meter-scale elliptical bodies dispersed in both rock types.

3 Sample description and petrography

From the Vysoký Kámen stock we have selected five samples of the leucogranite (20III, 20IV, 15B, 15C and 15D), one of the layered granite with UST (20II), three of the feldspathized leucogranite (20I, 20VII and 15A) and two of variously greisenized leucogranite (20V and 20VI). Additionally, we present data from the Čistá type granite, the most fractionated among the main granite types of the KGB.

The leucogranite is composed mostly of albite ($An_{0–2}$), potassium feldspar, quartz and subordinate amounts of lithium mica and topaz. Fluorapatite, Nb–Ta–Ti oxides, fluorite and rare beryl represent accessories. Quartz-free alkali-feldspar syenite, composed almost exclusively of albite and potassium feldspar, forms subhorizontal layers and lenses with diffuse contacts. It consists of albite ($An_{0–2}$), potassium feldspar, accessory lithium mica and topaz. Fluorapatite, triplite, Nb–Ta–Ti oxides, zircon, xenotime-(Y), monazite-(Ce) and very rare Nb-bearing wolframite are accessories. The alkali-feldspar syenite was described as feldspathite in some papers (e.g., Breiter et al., 1999; Jarchovský, 2006) but this name does not agree with the magmatic nature of this rock. The local pegmatite dykes are formed by K-feldspar, quartz and lithium mica with some rare minerals (such as beryl, bertrandite or kolbeckite).

The intense late magmatic and postmagmatic alteration of topaz–albite leucogranite and alkali-feldspar syenite resulted in irregular feldspathization, greisenization and muscovitization of the two rock types. The greisenized leucogranite contains albite ($An_{0–3}$), potassium feldspar, lithium mica (protolithionite, Li 0.41–0.44 apfu, Fe/(Fe + Mg) 0.96–0.99), quartz and topaz. Fluorapatite and zircon are accessories. The amounts of rock-forming minerals vary much (albite 40–60 vol.%, K-feldspar 0–30 vol.%, lithium mica 10–40 vol.%, quartz 5–15 vol.%, topaz 0–10 vol.%). The two greisenized samples differ in the amount of newly formed lithium mica, quartz, topaz and K-feldspar. The sample 20V contains topaz, less lithium mica and more quartz. The sample 20VI is characterized by the higher modal content of lithium mica and absence of K-feldspar. The NNW–SSE trending quartz–fluorite vein mineralization hosted by topaz–albite leucogranites and alkali-feldspar syenites resulted from the youngest hydrothermal activity in the area. A new generation of fine-grained feldspars (mainly albite) and white mica (muscovite) occurs in the feldspathized leucogranites.

4 Geochemistry

After the conventional crushing and homogenization of large fresh samples, the powders produced using agate mill have been analyzed for the whole-rock composition in Acme Analytical Laboratories Ltd., Vancouver, using the methods Geo3 (4A+4B) and 1DX. The major and minor elements were determined by ICP-OES and most trace elements by ICP-MS. The dissolution of the rock powders in dilute HNO_3 in both cases followed fusion with a $LiBO_2/Li_2B4O_7$ flux. Loss on ignition (LOI) is by weight difference after ignition at 1000 °C. The analyses of remaining trace elements, mostly transition metals (Mo, Cu, Pb, Zn, Ni, As, Cd, Sb and Bi), were carried out by ICP-MS following hot Aqua Regia digestion.

The studied rock types range from Tpz–Ab granite (Čistá type), through alkali granite (Tpz–Ab leucogranites from the Vysoký Kámen stock), to alkali-feldspar syenite (Fig. 2a). The studied lithologies are all poor in mafic cations and distinctly peraluminous, classifying as felsic peraluminous granitoids (f-P) sensu Villaseca et al. (1998) (Tab. 1).

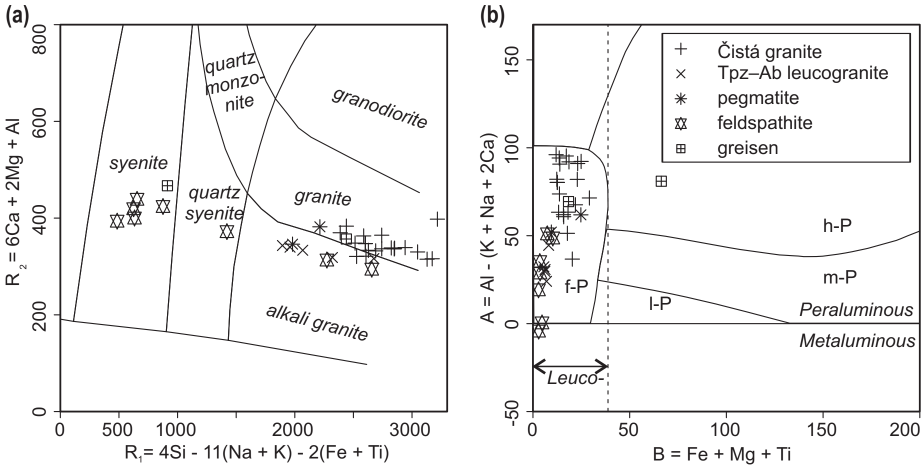

Fig. 2 *Multicationic classification diagrams for the Čistá (leuco-) granite and other granitic rock types from the Vysoký Kámen quarry. (a) R1–R2 plot (De La Roche et al., 1980), (b) B–A plot (Debon and Le Fort, 1983) modified by Villaseca et al. (1998). l-P: low-peraluminous, m-P: moderately peraluminous, h-P: highly peraluminous, f-P: felsic peraluminous*

The chondrite (Boynton, 1984) normalized REE patterns (Fig. 3a) are highly fractionated, with fairly low total REE contents (6.4–64.5 ppm in Čistá, 3.3–19.9 ppm the remaining rock types), rather flat (La_N/Yb_N = 1.13–3.82 for Čistá, 1.12–4.05 for the remaining rock types) with deep negative Eu anomalies (Eu/Eu* = 0.03–0.71for Čistá, 0.02–0.67 for the other rocks). A notable feature is the presence of M-type tetrad effect (Masuda et al., 1987). Its magnitude was expressed by the parameter TE_{1-3} (Irber, 1999), as calculated in the geochemical plotting package *GCDkit 3.0 beta* (Janoušek et al., 2006, 2011) by the plugin module *tetrad()* (Tab. 3). For the newly acquired analyses, where the quality and comparability of the data can be guaranteed, it ranges from 1.12 to 1.47 (pegmatite dyke KRU 15-II), roughly positively correlating with the increasing silica contents.

Two largely independent alteration processes, related to chemically different fluids, have been recognized in the southern part of the KGB: greisenization and feldspathization (Dolníček et al., 2012). The balance of trace elements in course of such transformations can be theoretically assessed using the multielement plot normalized by the least siliceous among our Čistá granite samples (KRU 22-I) (Fig. 3b; see also Tab. 2–3). Apparently, during feldspathization, many elements decreased in concentration (Cs, Th, U, REE); significant enrichments seem to be shown, in particular, by Ba and Sr. Greisenization results in increases in Cs, Rb and Sr contents; Th, U, Nb and REE seem also, to some extent, depleted.

However, the correct treatment of mass balance during open system-processes needs to take into account the changes in overall mass/volume of the whole system, which would also apparently alter the concentrations of immobile elements, whose abundances in reality did not change at all. Wedge diagrams (Ague, 1994), as implemented in the *GCDkit*, enable qualitative treatment of losses/gains of geochemical species during open-system geological processes, including hydrothermal alteration. As such they represent a viable alternative to the isocon plots (Grant, 1986, 2005) or concentration ratio diagrams (Ague, 1994), being in fact superior in that they take into account the overall variability of the whole dataset (both of the putative protolith and the altered product) and not just a selected whole-rock pair, and do not introduce any subjective

Table 1 Major-element data for the Čistá leucogranite and altered rock types from the Vysoký Kámen quarry(wt. %)

	KRU-22/I	**KRU-24/I**	**KRU-21/I**	**KRU-20/VI**	**KRU 15-II**	**KRU-20/III**	**KRU-20/V**
Locality	summit 792 W of Špičák	Milířský potok valley	Roník stock	Vysoký kámen	Vysoký kámen	Vysoký kámen	Vysoký kámen
Rock	Čistá granite	Čistá granite	Čistá granite	greisenized leucogranite	pegmatite dyke	granite	greisenized leucogranite
SiO2	73.98	74.49	75.12	61.54	70.40	72.32	72.34
TiO2	0.04	0.05	0.06	0.04	0.06	0.04	0.03
Al2O3	14.65	14.45	13.84	19.60	15.95	15.60	15.29
FeOt	0.97	0.97	1.59	4.54	1.49	0.33	1.13
MnO	0.06	0.05	0.10	0.22	0.08	0.02	0.07
MgO	0.07	0.07	0.08	0.11	0.13	0.04	0.09
CaO	0.28	0.32	0.37	0.72	0.25	0.33	0.49
Na2O	3.61	3.67	3.29	6.28	2.62	4.65	3.22
K2O	4.66	4.37	2.82	3.54	7.42	5.39	5.14
P2O5	0.31	0.30	0.32	0.59	0.32	0.43	0.33
LOI	1.20	1.10	2.20	2.20	1.10	0.80	1.70
Σ	99.83	99.84	99.79	99.38	99.82	99.95	99.83
K2O/Na2O	1.29	1.19	0.86	0.56	2.83	1.16	1.60
A/CNK	1.28	1.27	1.52	1.27	1.25	1.11	1.30
mg#	11.38	11.38	8.22	4.15	13.43	17.64	12.40
	KRU-20/II	**KRU 15-V**	**KRU 15-I**	**KRU-20/IV**	**KRU 15-IV**	**KRU 15-III**	**KRU-20/I**
Locality	Vysoký kámen	Vysoký kámen	Vysoký kámen	Vysoký kámen	Vysoký kámen	Vysoký kámen	Vysoký kámen
Rock	layered granite with UST	Znw-bearing leucogranite	Znw-bearing leucogranite	Znw-bearing leucogranite	Znw-bearing leucogranite	feldspathized leucogranite	feldspathized leucogranite
SiO2	72.54	72.79	73.15	74.95	75.62	71.68	75.87
TiO2	0.02	0.04	0.04	0.04	0.02	0.04	0.02
Al2O3	15.86	15.48	15.16	14.18	13.83	17.09	14.23
FeOt	0.58	0.34	0.26	0.36	0.37	0.12	< 0.04
MnO	0.05	0.03	0.03	0.02	0.03	0.02	0.02
MgO	0.05	0.04	0.06	0.06	0.11	0.03	0.02
CaO	0.64	0.32	0.31	0.35	0.37	0.33	0.31
Na2O	5.11	4.72	4.43	5.27	4.25	9.29	5.98
K2O	3.36	5.14	5.23	3.37	3.60	0.21	2.80
P2O5	0.69	0.47	0.46	0.40	0.37	0.27	0.40
LOI	1.00	0.60	0.90	1.00	1.40	0.90	0.70
Σ	99.90	99.97	100.03	100.00	99.97	99.98	100.35
K2O/Na2O	0.66	1.09	1.18	0.64	0.85	0.02	0.47
A/CNK	1.20	1.11	1.12	1.10	1.20	1.06	1.06
mg#	13.40	17.26	29.07	22.91	34.71	31.37	–

aspects, such as arbitrary scaling.

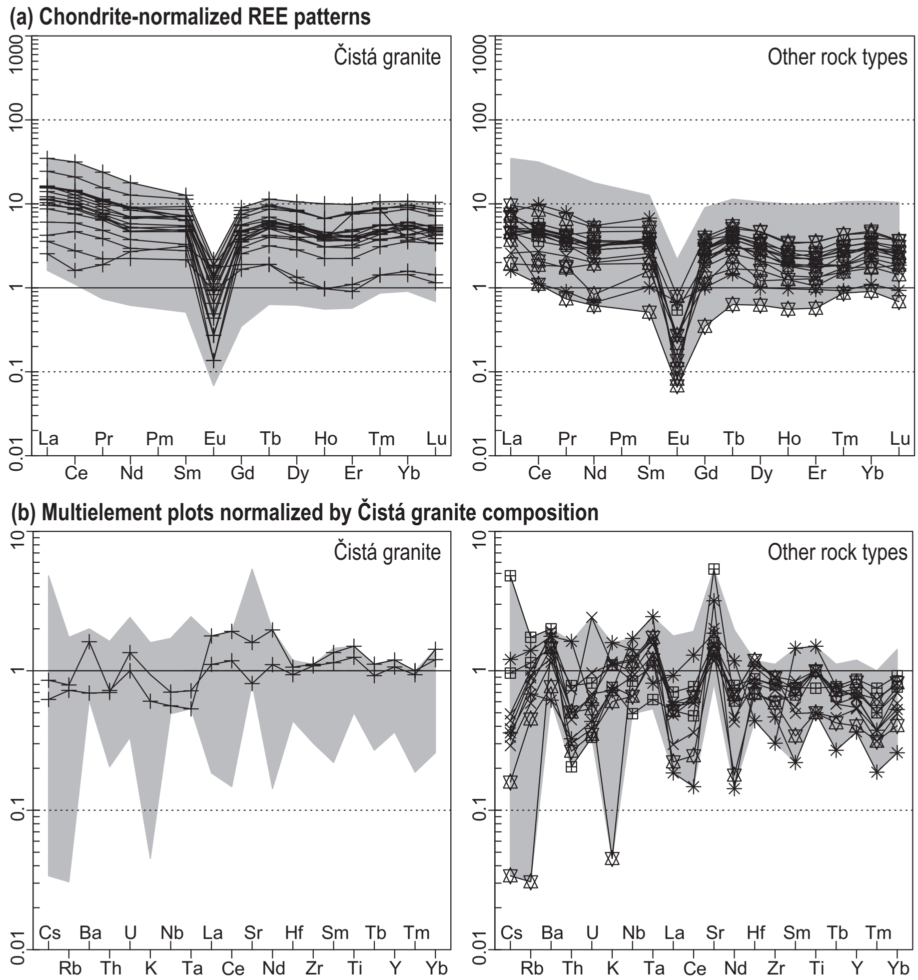

Fig. 3 *(a) Chondrite- (Boynton, 1984) normalized REE patterns. (b) Multielement plots normalized by the least siliceous Čistá granite KRU 22I.*

Wedge diagrams are binary plots of a potentially mobile element j versus a reference (immobile) element *i*. The compositionally heterogeneous protolith samples yield a cloud of points, the outer edges of which define a wedge-shaped region that converges towards the origin. As shown by Bucholz and Ague (2010), the altered samples that plot above and to the left of this wedge should have gained the mobile species, whereas those falling below and to the right suffered its loss. The samples that remain in the wedge but moved upwards are thought to record residual enrichment, and those shifted downwards to have undergone a residual dilution.

Table 2 Trace-element data except REE + Y for the Čistá leucogranite and altered rock types from the Vysoký Kámen quarry (ppm, Au in ppb)

	KRU-22/I	**KRU-24/I**	**KRU-21/I**	**KRU-20/VI**	**KRU 15-II**	**KRU-20/III**	**KRU-20/V**
Locality	summit 792 W of Špičák	Milířský potok valley	Roník stock	Vysoký kámen	Vysoký kámen	Vysoký kámen	Vysoký kámen
Rock	Čistá granite	Čistá granite	Čistá granite	greisenized leucogranite	pegmatite dyke	granite	greisenized leucogranite

Table 2 Trace-element data except REE + Y for the Čistá leucogranite and altered rock types from the Vysoký Kámen quarry (ppm, Au in ppb)

Rb	1144.2	828.2	905.4	1989.3	1599.8	1019.4	1309.0
Cs	118.1	73.6	101.0	567.0	142.5	45.4	113.7
Ba	13	9	21	26	23	25	19
Sr	7.9	6.4	12.6	42.4	14.7	10.8	12.6
Be	15	14	1	11	22	9	6
Ga	33.1	30.2	32.9	73.2	38.5	34.1	34.3
Sn	97	39	126	64	44	13	29
W	29.5	14.1	18.4	12.7	26.6	4.0	13.3
Nb	39.4	27.7	22.1	19.4	55.8	38.4	33.2
Ta	13.5	9.7	7.2	8.4	11.0	21.1	14.7
Zr	28.1	30.5	31.3	17.0	8.5	21.9	22.3
Hf	1.6	1.5	1.7	1.1	0.7	1.4	1.4
Th	8.3	5.8	6.0	1.7	13.5	4.1	6.5
U	6.0	8.1	6.0	2.0	3.4	3.9	4.9
Cu	1.3	1.4	17.3	3.4	3.8	3.8	3.6
Pb	2.2	3.2	0.8	1.0	2.1	1.7	1.9
Zn	54	20	21	221	70	13	68
As	3.3	1.5	0.7	1.9	4.8	2.4	7.7
Au	< 0.5	< 0.5	1.3	2.7	1.4	1.5	< 0.5
Bi	8.3	11.1	1.5	0.2	70.3	1.4	10.4
Sc	3	4	2	4	5.6	2	3
Cr	–	–	–	–	3	–	–
Ni	0.3	0.6	0.7	1.3	1.8	0.9	1.2
Co	< 0.1	< 0.1	0.2	0.8	0.5	< 0.1	< 0.1
V	< 8	< 8	< 8	< 8	< 2	< 8	< 8
	KRU-20/II	**KRU 15-V**	**KRU 15-I**	**KRU-20/IV**	**KRU 15-IV**	**KRU 15-III**	**KRU-20/I**
Locality	Vysoký kámen	Vysoký kámen	Vysoký kámen	Vysoký kámen	Vysoký kámen	Vysoký kámen	Vysoký kámen
Rock	layered granite with UST	Znw-bearing leucogranite	Znw-bearing leucogranite	Znw-bearing leucogranite	Znw-bearing leucogranite	feldspathized leucogranite	feldspathized leucogranite
Rb	779.0	1059.8	1156.3	669.8	902.3	35.1	516.0
Cs	42.4	51.9	58.0	34.3	39.4	4.0	18.8
Ba	8	16	23	15	19	19	10
Sr	25.1	12.4	9.4	10.8	15.9	11.2	10.5
Be	4	5	5	1	4	3	5
Ga	39.9	36.7	36.7	31.4	37.8	37	34.9
Sn	7	23	16	12	19	17	5
W	9.7	2.3	1.6	4.3	0.5	0.3	2.3
Nb	67.3	46.3	47.8	35.8	25.8	45.9	25.9
Ta	33.0	22.5	24.2	17.3	17.3	23.4	16.2
Zr	13.1	22.7	25.5	20.4	25.1	25.0	16.5
Hf	1.3	1.7	1.9	1.3	1.8	1.9	1.1
Th	2.7	4.3	6.1	3.7	2.5	4.2	2.2
U	2.6	14.5	5.8	4.1	2.3	3.2	2.1

Table 2 Trace-element data except REE + Y for the Čistá leucogranite and altered rock types from the Vysoký Kámen quarry (ppm, Au in ppb)

Cu	11.9	3.2	3.8	3.8	2.1	1.7	12.1
Pb	1.3	3.5	2.3	1.5	1.1	1.3	1.2
Zn	24	11	14	16	9	3	3
As	3.2	6.7	5.6	2.7	5.8	0.9	5.2
Au	1	1.5	1.5	< 0.5	1.3	0.6	0.8
Bi	0.2	2.3	0.2	0.2	0.2	1.3	< 0.1
Sc	1	0.7	3.5	2	0.4	0.7	< 1.0
Cr	–	2	1	–	2	1	–
Ni	2.1	0.9	0.8	1.6	1	0.6	2.3
Co	< 0.1	< 0.1	< 0.1	< 0.1	0.3	0.1	< 0.1
V	< 8	< 2	< 2	< 8	< 2	< 2	< 8

Selected Wedge plots are shown in Fig. 4. Regarding the major and minor elements, both modes of alteration are connected with influx of Al and Na (albitization) as well as P. Moreover, greisenization brings about also enrichment in ferromagnesian components, as well as Mn and Ca, while feldspathization leads to decrease in Fe ± Mn, and increase in K. Titanium, bound mostly to rutile and columbite group minerals (René and Škoda 2011), escaped unscathed. In terms of trace elements, most notable are enrichments in Rb, Cs, Sr and Zn, connected with greisenization; additionally, Rb was introduced in course of feldspathization, but without any significant Cs. On the other hand, the Wedge plots rule out any perceptible mobility of Ba, radioactive elements U and Th, Nb + Ta, as well as REE.

Table 3 Y + REE data for the Čistá leucogranite and altered rock types from the Vysoký Kámen quarry (ppm)

	KRU-22/I	**KRU-24/I**	**KRU-21/I**	**KRU-20/VI**	**KRU 15-II**	**KRU-20/III**	**KRU-20/V**
Locality	kóta 792 Z Špičáku	údolí Milířského potoka	peň Roník	Vysoký kámen	Vysoký kámen	Vysoký kámen	Vysoký kámen
Rock	Čistá granite	Čistá granite	Čistá granite	greisenized leucogranite	pegmatite dyke	granite	greisenized leucogranite
Y	7.7	8.2	9.2	5.4	4.9	5.3	6.7
La	2.7	3.0	4.8	1.4	2.5	1.6	1.9
Ce	6.1	7.2	11.7	2.9	7.9	3.6	4.7
Pr	0.78	0.86	1.38	0.38	0.96	0.47	0.58
Nd	2.8	3.1	5.5	1.7	3.3	1.9	2.2
Sm	0.91	1.04	1.23	0.61	1.32	0.70	0.69
Eu	0.02	0.02	0.07	0.04	< 0.02	< 0.02	< 0.02
Gd	0.98	0.97	1.21	0.52	0.97	0.66	0.75
Tb	0.26	0.24	0.29	0.17	0.20	0.18	0.20
Dy	1.56	1.29	1.73	0.67	1.00	0.94	1.07
Ho	0.27	0.29	0.33	0.13	0.13	0.16	0.20
Er	0.78	0.76	0.84	0.33	0.37	0.47	0.57
Tm	0.16	0.15	0.16	0.08	0.06	0.10	0.12
Yb	0.89	1.27	1.07	0.68	0.47	0.72	0.82
Lu	0.15	0.17	0.16	0.07	0.06	0.09	0.12

Table 3 Y + REE data for the Čistá leucogranite and altered rock types from the Vysoký Kámen quarry (ppm)							
ΣREE	18.36	20.36	30.47	9.68	19.24	11.59	13.92
LaN/YbN	2.045	1.593	3.024	1.388	3.586	1.498	1.562
LaN/SmN	1.866	1.815	2.455	1.444	1.191	1.438	1.732
Eu/Eu*	0.07	0.06	0.18	0.22	–	–	–
YbN	4.26	6.08	5.12	3.25	2.25	3.45	3.92
TE1-3	1.255	1.172	1.186	1.190	–	–	–
	KRU-20/II	**KRU 15-V**	**KRU 15-I**	**KRU-20/IV**	**KRU 15-IV**	**KRU 15-III**	**KRU-20/I**
Locality	Vysoký kámen	Vysoký kámen	Vysoký kámen	Vysoký kámen	Vysoký kámen	Vysoký kámen	Vysoký kámen
Rock	layered granite with UST	Znw-bearing leucogran-ite	Znw-bearing leucogran-ite	Znw-bearing leucogran-ite	Znw-bearing leucogran-ite	feldspathized leucogran-ite	feldspathized leucogran-ite
Y	2.8	5.0	5.7	4.2	4.1	6.4	3.1
La	0.5	1.3	1.6	1.5	0.8	1.4	0.6
Ce	0.9	3.8	4.0	3.6	2.2	4.0	1.5
Pr	0.11	0.44	0.51	0.40	0.29	0.50	0.22
Nd	0.4	1.7	1.9	1.3	1.2	1.9	0.5
Sm	0.20	0.61	0.77	0.50	0.45	0.67	0.31
Eu	0.05	< 0.02	< 0.02	0.02	0.02	< 0.02	0.02
Gd	0.26	0.60	0.74	0.53	0.46	0.74	0.29
Tb	0.07	0.15	0.18	0.15	0.12	0.19	0.11
Dy	0.32	0.84	0.95	0.80	0.68	1.10	0.39
Ho	0.07	0.13	0.17	0.14	0.10	0.17	0.09
Er	0.20	0.40	0.45	0.38	0.28	0.53	0.22
Tm	0.03	0.06	0.08	0.06	0.05	0.10	0.05
Yb	0.23	0.52	0.62	0.62	0.44	0.73	0.36
Lu	0.03	0.07	0.08	0.09	0.05	0.10	0.06
ΣREE	3.37	10.62	12.05	10.09	7.14	12.13	4.72
LaN/YbN	1.466	1.685	1.740	1.631	1.226	1.293	1.124
LaN/SmN	1.573	1.341	1.307	1.887	1.118	1.314	1.217
Eu/Eu*	0.67	–	–	0.12	0.13	–	0.20
YbN	1.10	2.49	2.97	2.97	2.11	3.49	1.72
TE1-3	1.119	–	–	1.324	1.320	–	1.468

5 Magnetic fabric and magnetic properties

The detailed rock-magnetic analyses were conducted in order to study the changes in magnetic properties associated with two alteration processes in the granite. It has included the measurements of thermomagnetic properties, the hysteresis loops, curves of acquisition of isothermal remanent magnetization (IRM), direct-field remagnetization (DCD) curves and anisotropy of magnetic susceptibility (AMS).

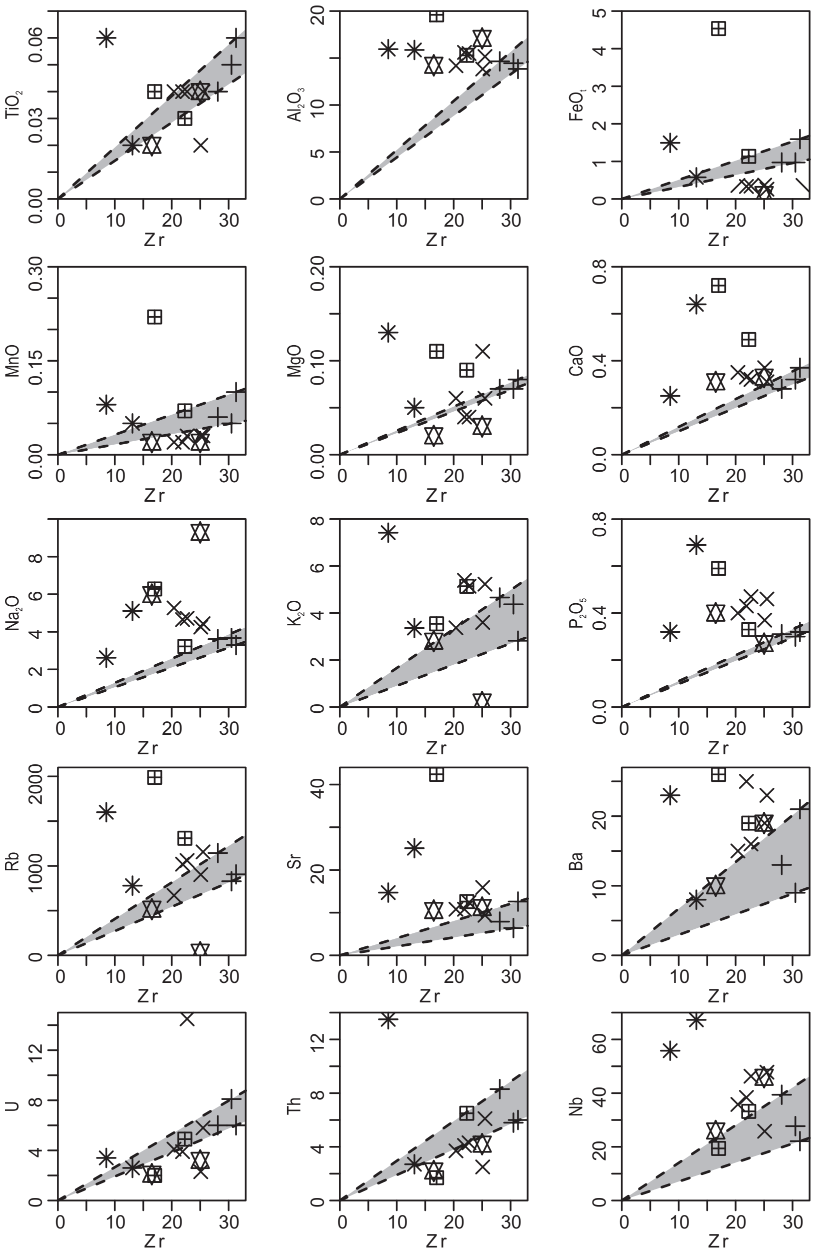

Fig. 4 *Selected Wedge diagrams (Ague, 1994; Bucholz and Ague, 2010) for the Čistá type granites (crosses) taken as the likely protolith to the other, variously altered rocks from the Vysoký Kámen quarry (symbols as in Fig. 2). Wedge diagrams are binary plots of a potentially mobile geochemical species versus a reference (immobile) element (here Zr). Major- and minor-element oxides in wt. %, trace elements in ppm. For explanation, see the text.*

5.1 Magnetic mineralogy

The magnetic mineralogy is studied by a combination of measurement of magnetic susceptibility changes with temperature and the hysteresis loops, IRM and DCD curves. The measurements of thermomagnetic curves were carried out on powder specimens using the CS-3 Furnace and/or the CS-L Cryostat Apparatus and the KLY-4S Kappabridge (Hrouda, 1994; Jelínek and Pokorný, 1997) at the Institute of Geophysics in Prague. Hysteresis and remanent parameters were measured by Vibrating Sample Magnetome-

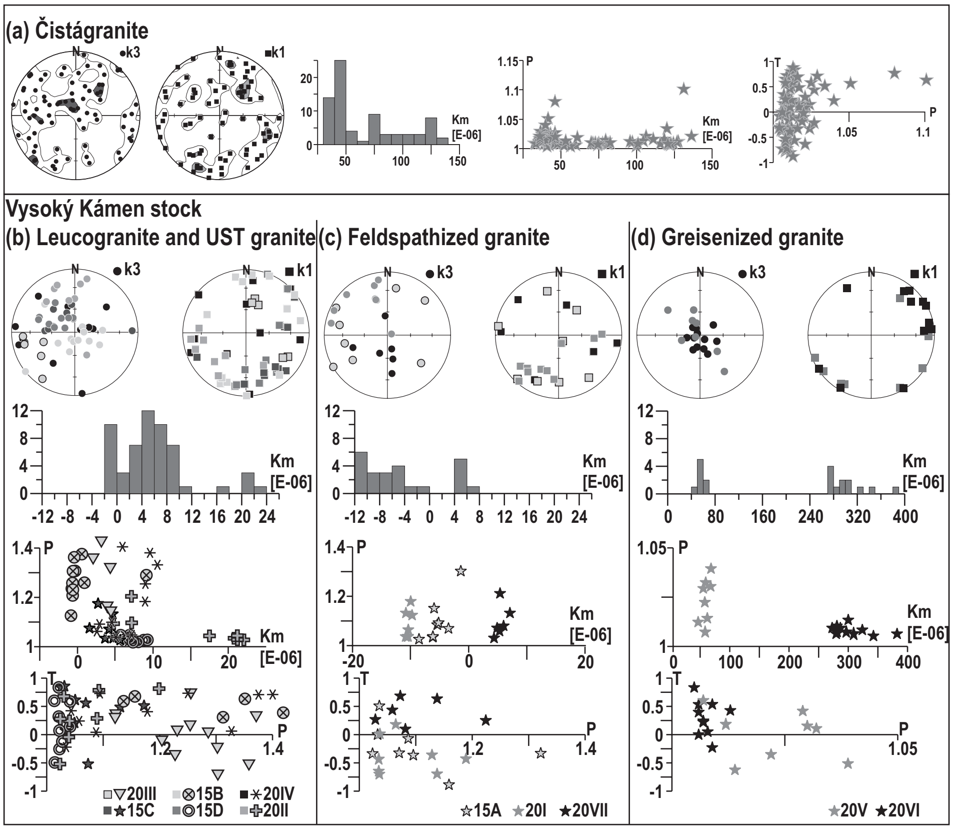

Fig. 5 *Summarizing figure of magnetic results showing the mean magnetic susceptibility(Km) , P–T diagram, representing degree and shape of AMS and AMS orientation in a) Čistá granite and in granites of Vysoký Kánem Stock: b) leucogranites and UST granite, c) feldspathized leucogranites and in d) greisenized leucogranites.*

ter (Model EV9 VSM, DSM Magnetics; ADE Corporation, Lowell, MA, USA) also at the Institute of Geophysics in Prague.

Magnetic susceptibility

The host of the Vysoký Kámen stock, the most fractionated of the main granite types of the KGB, the Čistá granite shows magnetic susceptibility values in the range from 32.5^{-06} to 136.4^{-06} [SI] with the median of 46.3^{-06} [SI] (Fig. 5a)

The leucogranite, feldspathized leucogranite and granite with UST of the Vysoký Kámen stock reveal very low mean bulk magnetic susceptibility (Km) oscillating around zero (Fig. 5b,c). The Km of the leucogranites ranges from -0.9×10^{-6} to 22×10^{-6} [SI] with the median of 4.9. There are two subgroups within the leucogranite samples with the median values 19.2 and 4.6 respectively. The Km of the feldspathized leucogranite ranges from -10.9×10^{-6} to 7×10^{-6} [SI], with the median value of -6 suggesting the dominance of diamagnetic minerals. In contrast, the Km of the greisenized leucogranites (Fig. 5d) shows higher values, the sample 20V with less mica has median value 55 $\times 10^{-6}$ [SI] and sample 20VI exhibits higher medium value 296 $\times 10^{-6}$ [SI].

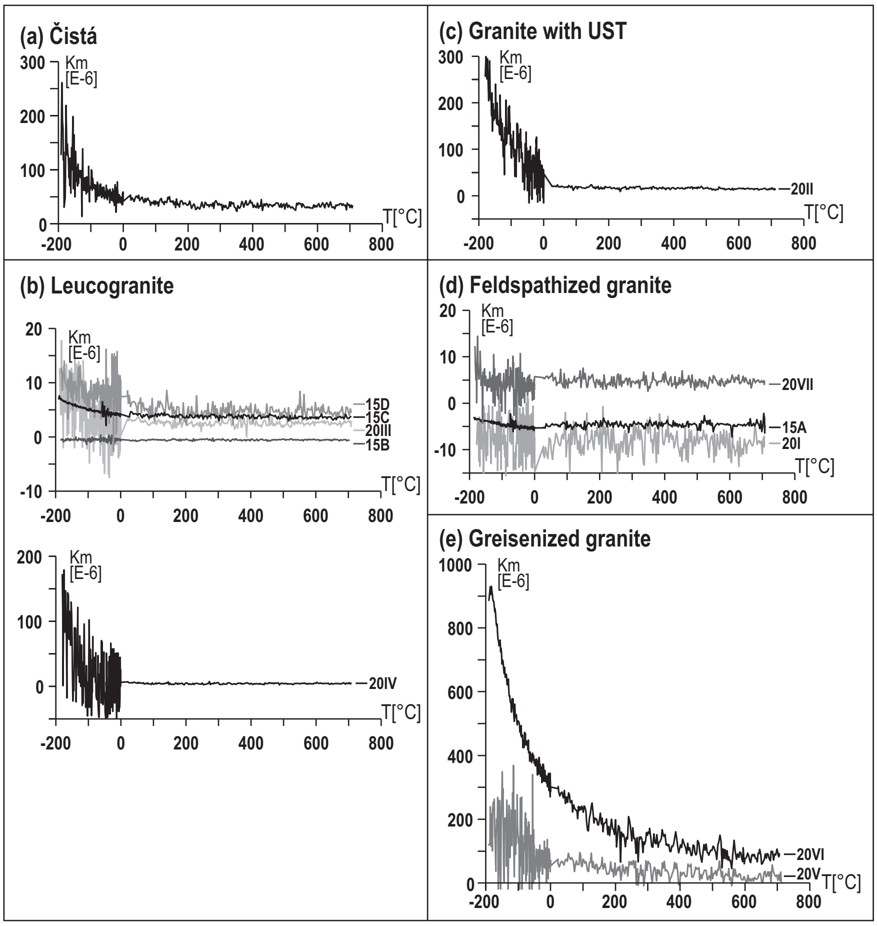

Fig. 6 *Thermomagnetic curves showing the a) the Čistá granite, b) the leucogranite samples, c) the layered granite with UST, d) the feldspathized leucogranites, e) the greisenized leucogranites.*

Thermomagnetic curves

The thermomagnetic curve of the Čistá granite (Fig. 6a) is hyperbolic in shape suggesting the dominant contribution of paramagnetic phases. The leucogranites show two main behavior types of magnetic susceptibility (Fig. 6b). The sample 15D reveals linear and the rest of the leucogranite samples yield hyperbolic patterns, in particular at low temperatures. The layered granite with UST exhibits important decrease in Km at low-temperature range and constant Km above 0°C (Fig. 6c). The thermomagnetic curve of the feldspathized leucogranite 20VII exhibits constant negative trend typical of the diamagnetic behavior (Fig. 6d). The others show slight decrease in Km at low temperatures. The thermomagnetic curves of the greisenized samples reveal hyperbolic decay (Fig. 6e), indicating an importance of paramagnetic phases.

Hysteresis loops, IRM and DCD curves

The hysteresis loops, isothermal remanent magnetization acquisition (IRM) curves and DC remagnetization (DCD) curves were measured (in the range from -2000 mT to 2000 mT or from -1000 mT to 1000 mT) on crushed samples and fragments in order to characterize the basic magnetic parameters.

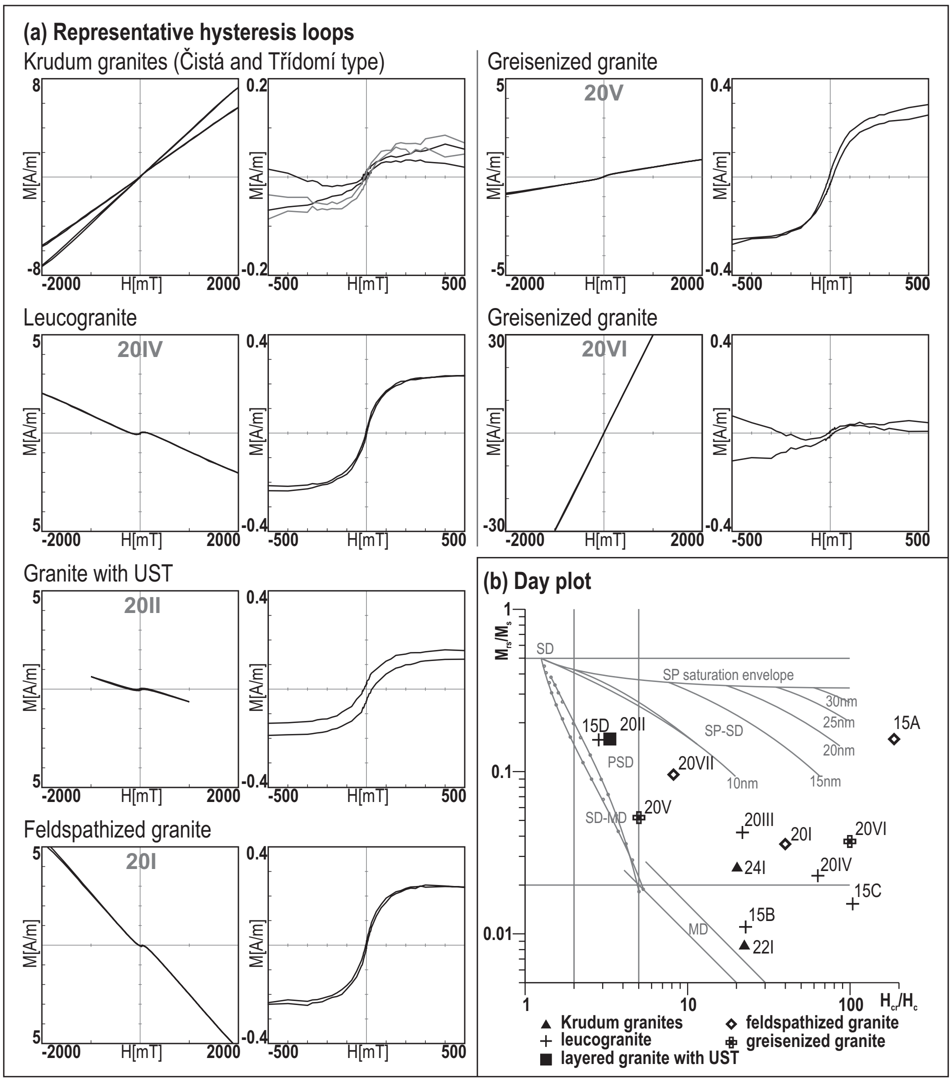

Fig. 7 *Hysteresis and remanence parameters. a) Representative hysteresis loops for each studied granite type, b) hysteresis and remanence parameter ratios Mr/Ms and Hcr/Hc plotted in Day plot with theoretical curves for magnetite acquired from Dunlop (2002).*

The measured hysteresis curves of leucogranites, UST granite and feldspathized leucogranites (Fig. 7a) are controlled by linear signal with negative slope, suggesting predominance of diamagnetic minerals. In contrast, ordinary granites from the KGB (the Čistá and Třídomí types) and greisenized granites show an overall paramagnetic character. After the correction for the dia/paramagnetic signal by subtracting the linear part of the hysteresis curves below -500 mT, weak ferrimagnetic component was revealed in all the samples (Fig. 7a).

The shape of the hysteresis curves of the ferrimagnetic component suggests the presence of magnetite and/or maghemite. Values of saturation magnetization (M_s), saturation remanence (M_r), coercivity (H_c) of hysteresis loop and remanent coercivity (H_{cr}) determined from measured DCD curves are summarized in Table 4. On the basis of the modified Day plot (Day et al., 1977, Dunlop, 2002) we assume that multi-domain (MD) character of magnetic particles prevails in the Krudum granites, most of leucogranites, greisenized samples and one feldspathized leucogranite (20I) (Fig. 7b). In contrary, two other samples of the feldspathized leucogranite show dominance of superparamagnetic (SP) particles but of significantly different grain size (Fig. 7b). The M_r/M_s and H_{cr}/H_c ratios in Day plot of one leucogranite (15D) and of the granite with UST (20II), suggests the presence of a significant amount of single-domain and/or pseudosingle-domain (PSD) particles (Fig. 7b).

Table 4 Summarized values of magnetic measurements

	M_S E-04 [emu/g]	M_{rs} E-05 [emu/g]	H_{cr} [Oe]	H_C [Oe]	H_{cr}/H_C []	M_{rs}/M_S []	χ_v E-06 [SI]	χ_{vd+p} E-06 [SI]	Mag ‰	χ_{vMag} E-06 [SI]
Krudum granites										
22I	10.64	0.89	664	29.7	22.36	0.008	48.33	4.59	0.18	0.027
24I	8.29	2.1	688	34.1	20.18	0.025	49.27	3.57	0.28	0.042
Leucogranites										
15B	26.05	2.87	230	10.1	22.77	0.011	-0.58	-1	2.81	0.415
15C	8.8	1.35	550	5.3	103.77	0.015	4.22	-1.59	0.91	0.136
15D	3.35	5.25	190	67	2.84	0.157	7.35	-0.97	0.32	0.048
20IV	5.51	1.26	1096	17.3	63.35	0.023	6.41	-1.44	0.51	0.077
20III	4.54	1.91	925	42.5	21.76	0.042	3.17	-1.19	0.47	0.07
Layered granite with UST										
20II	8.18	12.99	768	231	3.32	0.159	20.83	-1.07	0.76	0.117
Feldspathized granites										
15A	0.5	0.79	280	1.5	186.67	0.159	-5.19	-1.07	0.06	0.009
20I	4.16	1.49	834	20.9	39.9	0.036	-10.45	-3.46	0.46	0.068
20VII	2.66	2.55	500	61	8.2	0.096	5.39	-1.56	0.3	0.045
Greisenized leucogranites										
20V	21.85	11.37	451	89.9	5.02	0.052	64.01	1.43	1.97	0.299
20VI	9.92	3.68	558	5.6	99.64	0.037	294.53	18.59	0.16	0.025

Saturation magnetization (M_S), saturation remanence (M_{rs}), coercivity (H_C) of hysteresis loop, remanent coercivity (H_{cr}) and parameter ratios M_{rs}/M_S and H_{cr}/H_C for the Day plot, values of volume susceptibility measured measured by AC Kappabridge (χ_v), calculated values of susceptibility of diamagnetic + para-magnetic phases (χ_{vd+p}) recorded by the slope of linear part of hysteresis curve, volume of magnetite (Mag) and its susceptibility (χ_{vMag}) calculated from saturation of the hysteresis loops (for detailed explanation see text).

In attempt to quantify the influence of the inferred ferrimagnetic phase on magnetic susceptibility and its anisotropy, we have calculated the volume magnetic susceptibility of the diamagnetic + paramagnetic phases (χ_{vd+p}) in the samples recorded by the slope of linear part of hysteresis curve (Tab. 4). Results suggest that the diamagnetic + paramagnetic phases represent minor proportion of the bulk magnetic susceptibility (χ_v) measured by AC Kappabridge in all the samples (Tab. 4). This however, is in contrary to the shape of measured thermomagnetic curves, and shape and magnitude of the hysteresis curves of the ferrimagnetic component (Fig. 7a). This discrepancy is best observed in the case of greisenized granite 20VI, which exhibits calculated χ_{vd+p} value equal to 18.5 × 10-6 [SI], but the measured bulk susceptibility is 294.5 × 10-6 [SI]. The sample clearly shows pronounced hyperbolic shape of thermomagnetic curve (Fig. 6a) and the measurement disclosed only a very weak influence of ferrimagnetic phase on magnetic hysteresis of the sample (Fig. 7e). To shed light on this dissimilarity in different magnetic measurements, we have also calculated the volume magnetic susceptibility of ferrimagnetic phase (χ_{vMag}) (Tab. 4) based on saturation of the hysteresis loops, saturation magnetization and mass susceptibility of clear (100%) ferrimagnetic phase and density of samples (Tab. 5), assuming that the ferrimagnetic phase is magnetite. From the hysteresis loops saturation and saturation magnetization of magnetite (93 [Am^2kg^{-1}], Tarling and Hrouda, 1993) we have calculated proportion of them in samples (Tab. 4). From the proportion and mass susceptibility of magnetite (578 × 10-8 [SI/kg], Tarling and Hrouda, 1993) we calculate mass susceptibility and convert it to volume susceptibility using measured density of samples. The calculated volume of magnetite is ranging between 0.06 ‰ to 2.81 ‰ and the corresponding volume susceptibility (X_{vMag}) varies from 0.009 × 10^{-6} [SI] to 0.415 × 10^{-6} [SI]. The lowest values are observed in feldspathized leucogranites, unaltered KGB granites and greisenized granite with high mica abundance (Tab. 4). In contrast to the values of dia- and paramagnetic susceptibility, obtained from the linear slope of the hysteresis loops, the values of susceptibility represented by the ferrimagnetic phase, calculated from the saturation magnetization, suggest that the magnetic susceptibility and, consequently, the AMS is carried mainly by dia- and paramagnetic phases.

Analysis of hysteresis, IRM and DCD curves suggests the presence of ferrimagnetic phase(s) in all the samples, probably magnetite and/or maghemite. It also point to non single-domain nature of magnetic particles in most of the samples and the possibility of "inverse" AMS fabric (Rochette et al., 1999) can be excluded in these samples. The SD particles are expected within the leucogranite (15D) and granite with UST (20II), where the inverse fabric seems to be present in UST granite sample were AMS is at high angle to subhorizontal magmatic layering.

5.2 AMS fabric

The XY oriented samples were collected and studied in the laboratory. The AMS was measured with the KLY-4S Kappabridge (Jelínek and Pokorný, 1997) in the field of 300 A/m root-mean-square value in the Institute of Geophysics. The data were statistically evaluated using the Anisoft 4.2. package of programs (Jelínek, 1978; Hrouda et al., 1990; Chadima and Jelínek, 2008). The AMS ellipsoid was characterized by its intensity (indicated by the degree of anisotropy $P = k1/k3$ for samples with $Km>0$ and $P = |k3|/|k1|$ for samples with $Km<0$ as suggested by Hrouda (2004) and its symmetry (shape factor $T = 2ln(k1/k2)/ln(k2/k3)–1$, where $0<T<1$ constraints oblate and $-1<T<0$ prolate shapes of AMS ellipsoids). The principal magnetic susceptibilities are following $k1 \geq k2 \geq k3$.

The Čistá granite, the host of the Vysoký Kámen stock, encompasses subhorizontal, WNW–ESE and NE–SW trending fabrics with predominant steep ones. The AMS ellipsoids are characterized by low mean value of P parameter being 1.011 with a few outliers and prolate to oblate shapes (Fig. 5a).

The orientation of the magnetic fabrics in the leucogranite and UST granite samples is relatively scattered with two main directions (Fig. 5b), the quasi horizontal and the steep, NW–SE trending foliation. The majority of the lineations is distributed subhorizontally. The feldspathites also show two main types of fabrics (Fig. 5c). The wide cluster of the subhorizontal middle-angled foliation alternates with the NW–SE trending steep fabrics. The magnetic lineation exhibits preferential SW-dipping orientation. The samples from the greisenized granite (Fig. 5d) represent the best clustered results with the horizontal magnetic foliation bearing horizontal, NE–SW trending lineation. The sample 20V with less mica marked by grey circles is more scattered than the sample 20VI with higher mica contents.

The degree of magnetic anisotropy (P parameter) is in leucogranites relatively low (median for P = 1.093). The shape of the AMS ellipsoid changes from highly prolate (minimal T = -0.74) to highly oblate (maximal T = +0.84), with the median value in plane-strain to slightly oblate region (T = 0.28). In feldspathized leucogranite, the P parameter is highly variable (1.024–1.857). The shape of AMS ellipsoid also covers the whole spectrum (T = -0.91 to +0.67) and the median value showing more prolate shape (T = -0.31). The samples from the greisenized granite shows low values of AMS intensity defined by P parameter from 1.005 to 1.039 with the median P = 1.01. The shape of AMS exhibits plane-strain symmetry (median T = 0.15) with the values ranging from -0.64 to +0.82.

There is a considerable problem in interpreting very low susceptibility samples especially from the leucogranite and feldspathite groups. These samples show Km close to zero (median Km = 4.9 and -6). Hrouda (2004) demonstrated the unrealistically high values of degree of AMS in the vicinity of zero susceptibility. Based on modeling of quartzite and limestone AMS, he suggested to avoid the quantitative interpretation of AMS of rocks with the bulk magnetic susceptibility between -5×10^{-6} and 5×10^{-6} [SI]. In our data set, it concerns in particular the part of the leucogranite samples and all feldspathized leucogranite samples (Fig. 5b,c). The leucogranites out of the Km range suggested by Hrouda (2004) to be not interpreted in terms of P parameter are of low values up to 1.05.

6 Pore space characterization

Porosity and pore space character of Tpz–Ab leucogranites, feldspathized leucogranite and greisenized leucogranites from the Vysoký Kámen stock was determined using the mercury-injection porosimetry and the results was confronted with microstructural observations.

The mercury porosimetry initially proposed by Washburn (1921) provides a wide range of information, e.g. the pore size distribution, the total pore volume or porosity, the skeletal and apparent density. The technique is based on volume measurement of mercury forced into the porous sample by external pressure. The mercury pressure and the pore size are related by the Young–Laplace equation for the displacement of a non-wetting fluid in a thin capillary tube:

$$r = \frac{(-2\gamma cos\vartheta)}{p}$$

where r is the radius of the capillary tube, or the distance of the pore walls in slit-shaped pore (Lenormand et al., 1983), γ is the mercury surface tension (485 × 10-3 Nm-1), ϑ is the contact angle between the mercury and solid (130°), and p is the capillary pressure applied on the liquid. The pore throat size represents the largest connection (throat or pore channel) from the sample surface towards that pore and therefore is bigger than pore size determined by direct methods (Giesche, 2005). The measurements were performed at the University of Strasbourg on mercury-injection porosimeter Micromeritics AutoPore IV using 220 MPa as maximum mercury pressure and thus giving access to pores with throat diameter between 300 µm and 5 nm. To reveal the sample pore space geometry the mercury volume was measured during three stages of step-wise change of the applied pressure: (1) mercury intrusion by the pressure increase to the maximum; (2) mercury extrusion by the pressure release to the ambient pressure and (3) mercury reintrusion by the pressure returning to the maximum. The pore space volume of filled by mercury during the first stage is called total porosity. The volume of mercury remaining in the sample pore space after pressure release (second stage) is termed trapped porosity and is related to the heterogeneity of the network geometry (Li and Wardlaw 1986a, b; Wardlaw et al. 1987). The volume of mercury reintruding the pore space during the third stage is related to free porosity only. The results of mercury-injection porosimetry are presented as curves of incremental porosity vs. pore throat size calculated from intrusion pressure using the Washburn equation (Fig. 8) and in summarizing Table 5 showing values of total porosity, bulk and skeletal density and pore throat size, where the median corresponds to the pore throat size at which the mercury has filled a half of the pore space volume during the step-wise intrusion. The parameter characterizing the free-to-total porosity ratio is calculated by dividing the porosity volume of the reintrusion (stage 3) by the porosity volume of the first intrusion (stage 1).

The microstructure of all samples is in thin section scale homogenous and show no evidence of zones of altered and unaltered rock matrix. The qualitative evaluation of microporosity in thin sections of all studied samples regardless the rock type documents the dominant presence of intergranular microcracks mainly occuring in feldspars and on grain boundaries (supplementary Fig. S1). The granite types differ mainly in abundance of microcracks along grain boundaries of newly formed mica in greisenized leucogranites. In feldspathized leucogranites, smaller microcracks length associated with smaller grain size of feldspar crystals are newly formed by feldspathization process. In greisenized leucogranite, intergranular cracks also seem to be wider in comparison to other studied granite types.

6.1 Leucogranite and granite with UST

The curves of incremental porosity for the leucogranite samples are characterized by wide peak and different pore size of free and trapped porosity (Fig. 8a). Values of total porosity range in narrow interval between 0.9 and 1.7 % with free/total porosity ratio between 18 and 31 % (Tab. 5). All samples show similar values of bulk and skeletal density being 2.58 and 2.61 gcm^{-3} in average. The median pore throat size is 0.25 μm in average ranging between 0.19 to 0.35 μm.

The sample of layered granite with UST shows among non-altered samples exceptionally low total porosity (0.7 %) and free/total (11 %) porosity ratio as well as pore throat size (0.07 μm) (Tab. 5). It also differs in higher bulk and skeletal density (2.67 and 2.68 gcm^{-3}, respectively).

6.2 Feldspathized leucogranite

The two feldspathized leucogranite samples (20I and 15A) show similar values of total porosity and density compared to the leucogranite samples, but differs in significantly lower free/total porosity ratio (13 and 14 %) and absence of the wide peak on total porosity curve (Fig. 8b). The less porous sample 15A (0.7 %) also shows significantly smaller pore throat size, 0.08 μm. The third measured sample (20VII) exhibits distinct results from other two feldspathized leucogranite as well as from the leucogranites. It is characterized by high porosity (2.8 %) with high free/total porosity ratio (41 %) and relatively high pore throat size and low bulk density.

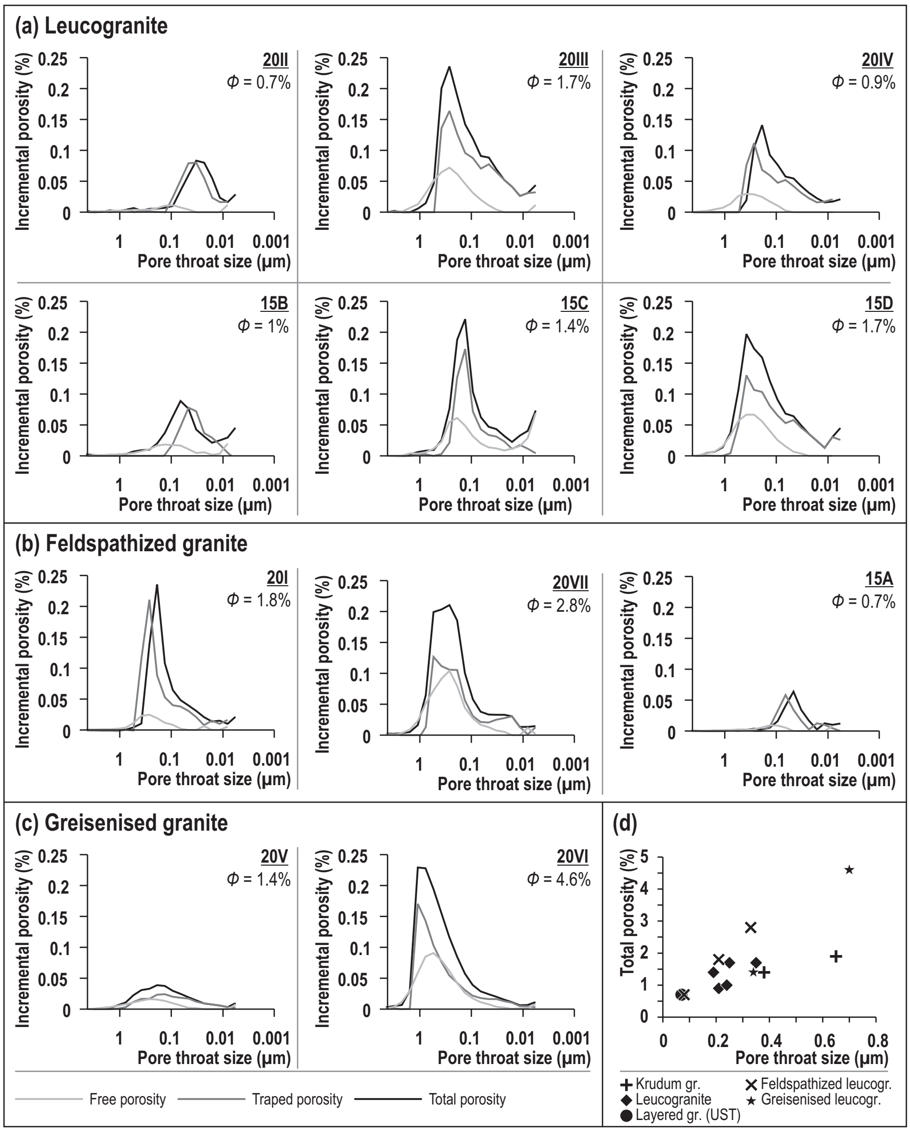

Fig. 8 *Results of mercury-injection porosimetry of a) leucogranite and granite with UST, b) feldspathized leucogranites and c) the greisenized leucogranites. d) graph of relation between pore throat size and porosity.*

6.3 Greisenized leucogranite

Two samples of differently greisenized leucogranite were characterized by the mercury porosimetry. The sample 20V with smaller mica amount exhibits similar porosity characteristics as the studied leucogranites with most of the values at the upper limit of the leucogranites range and a slightly higher skeletal density value (Fig. 8c and Tab. 5). The other sample 20VI with more newly formed mica, shows significant increase in porosity (4.6 %), free/total porosity ratio (38 %), pore throat size (0.7 μm) and skeletal density 2.76 gcm^{-3}, although the bulk density (2.63 gcm^{-3}) is the same as for the less altered sample and close to the values obtained for the leucogranites.

7 Summary and discussion

7.1 Geochemical evolution during alteration

Two largely independent alteration processes, related to chemically different fluids, can be recognized in the Vysoký Kámen stock, greisenization and feldspathization.

The greisenization was caused by near-critical low-salinity aqueous fluids with low contents of CO_2, CH_4, and N_2 (= 10 mol. % in total) at ~350–400 °C and 300–530 bar (Dolníček et al., 2012). The influx of these fluids led to an enrichment in Fe, Mn, Al, Na, F, Sn, W, Rb, Cs, Sr and Zn. At more advanced stages, Nb, Ta and LREE became also elevated. The fluid activity continued even after greisenization, and was connected with feldspathization and later argillitization as documented by abundant secondary fluid inclusions. These inclusions reflect the whole cooling history down to c. 50 ºC (Dolníček et al., 2012). The hydrogen (δD = -70 to 81 ‰ SMOW) and oxygen ($\delta^{18}O$ = +10.4 to 10.6 ‰ SMOW) isotope data collected from altered rocks have been, however, interpreted in terms of interaction of granite with meteoric waters under post-magmatic conditions (Dolejš and Štemprok 2001).

The other characteristic fluid-related feature is the occurrence of tetrad effect in chondrite-normalized REE patterns (Dolejš and Štemprok, 2001; see also Fig. 3a). Most of the workers nowadays agree that the occurrence of M-type lanthanide tetrad effect is connected to fluorine-rich environments, being caused by melt/fluid (Irber, 1999; Monecke et al., 2002; Zhao et al., 2002) or melt/melt fractionation (Veksler et al., 2005).

The greisenized samples from the Vysoký Kámen stock, if compared to leucogranite and feldspathized leucogranite, are clearly enriched in Fe, Mn and Zn, i.e. elements triggering paramagnetism of minerals (Fig. 4). In contrast, the feldspathization resulted in depletion of the same mafic cations. These were most likely leached by the fluid derived from the decomposing Li-micas (protolithionite). In turn, a new generation of feldspars (mainly albite) and muscovite grew from the newly introduced components; the same process presumably resulted in the formation of the quartz–hematite veins.

It has to be stressed that the studied samples represent rather incipient stages of the alteration processes, especially of greisenization, eventually leading to economic Sn–W deposits of the Krásno area. Perhaps for this reason we have not recorded any significant depletions/enrichments of U, Th, Nb, Ta or REE, which were demonstrated to be mobile in Cl, F-rich hydrothermal fluids (Alderton et al., 1980; Witt et al., 1988; Keppler and Wyllie, 1990; Rubin et al., 1993). This, together with the arguably more objective approach (Wedge plots vs. isocons) without the necessary arbitrary scaling and an assumption of conserved volume, may account for some differences if compared with the previous study of Dolejš and Štemprok (2001). For instance, these authors inferred addition of some Zr and Th, and removal of U, in course of greisenization but they did not have data to assess the cases of REE, Nb, and Ta.

7.2 Evolution of magnetic properties during alteration process

Primary leucogranites of the Vysoký Kámen stock are characterized by low magnetic susceptibility (median = 4.9×10^{-6} [SI]), paramagnetic character of thermomagnetic curves and by AMS orientation consistent with the general pattern in the Čistá granite and the whole KGB (Machek et al., 2011) (Figs 5,6). The hysteresis and remanent measurements reveal overall diamagnetic behavior with significant presence of a ferrimagnetic phase (probably magnetite and/or maghemite) of dominantly multi-domain character with tendency to superparamagnetic behavior (Fig. 7). If compared to the paramagnetic Krudum granites (the Čistá type), leucogranites of the Vysoký Kámen stock exhibit lower susceptibility, but higher proportion of ferrimagnetic phase (Fig. 5, 7, Tab. 4).

To decipher the influence of ferrimagnetic and diamagnetic + paramagnetic phases on the magnetic susceptibility and thus on the AMS, we performed calculation of the volume magnetic susceptibility of diamagnetic + paramagnetic phases (X_{vd+p}) in the samples recorded by the slope of linear part of hysteresis curve and the volume magnetic susceptibility of ferrimagnetic phase (X_{vMag}) based on saturation of the hysteresis loops (Tab. 4). Results based on slope of linear part of hysteresis curves suggest that the diamagnetic + paramagnetic phases represent minor proportion of the bulk magnetic susceptibility (X_v) measured by AC Kappabridge in all the samples. This however, this is contrary to the shape of measured thermomagnetic curves, shape and magnitude of the hysteresis curves and proportion of the ferrimagnetic component deduced from saturation magnetization. The calculated portion of magnetite is ranging between 0.06‰ to 2.81‰ and the corresponding volume susceptibility (X_{vMag}) varies from 0.009 $\times$ 10^{-6} [SI] to 0.415 $\times$ 10^{-6} [SI], which is suggesting that the magnetic susceptibility and consequently the AMS is carried mainly by dia and paramagnetic phases. It seem that the later mentioned calculation of volume susceptibility based on saturation magnetization is closer to the reality as it is in accordance with the observed shapes of thermomagnetic curves and hysteresis loops. The physical meaning of the dissimilarity of calculated volume susceptibility of ferrimagnetic and diamagnetic + paramagnetic phases and volume susceptibility measured by AC Kappabridge is unclear to us. The only questionable explanation, we can think of, may lay in different technical way of susceptibility measurements in low AC magnetic field at Kappabridge and high DC field at Vibrating Sample Magnetometer.

The feldspathization process even decrease already low susceptibility (median = -6 $\times$ 10^{-6} [SI]) (Fig. 5c) by increasing influence of diamagnetic phases and slightly decreasing the content of ferrimagnetic phase (Fig. 7a, Tab. 4), while preserving the AMS orientation. The geochemical analysis reveals that the feldspathization led to depletion in mafic cations and decomposition of Li-mica originally present in unaltered leucogranite, which can clarify the susceptibility decrease. Based on above mentioned results it seems, that the stability of the AMS orientation is due to insignificant influence of feldspathization process on orientation of paramagnetic and diamagnetic phases oriented during granitic magma emplacement.

Contrary to the feldspathization, the greisenization led in studied sample to significant change of magnetic properties. Considerably higher magnetic susceptibility (55 and 296 $\times$ 10^{-6} [SI]) than in leucogranites is produced mostly by paramagnetic phases (newly formed Li-mica), documented by thermomagnetic curves together with hysteresis loops (Figs 6,7). The subhorizontally oriented AMS is of low degree and plain-strain symmetry. The geochemically documented influx of elements during greisenization led to metasomatic growth of lithium mica, quartz, topaz and K-feldspar in granite microstructure and probably also to decomposition of fine-grained ferrimagnetic phase as suggested by its negligible influence on hysteresis loops (Fig. 7a, Tab. 4). By such fundamental change of microstructure the original AMS is completely reworked.

7.3 Development of porosity

Leucogranites as the primary granite type of the Vysoký Kámen stock exhibits relatively low porosity (0.9–1.7 %) with free/total porosity ratio ranging between 18 and 31 %, average pore throat size of 0.25 μm and average skeletal density 2.61 gcm-3. Such total porosity values are slightly higher than for fresh non-fractured granites (< 1 %) and correspond to values of only weakly altered and/or fractured granites (Nur and Simmons, 1969; Geraud et al., 1993; Surma and Géraud 2003; Rosener and Géraud, 2007; Staněk et al., 2013) and are in agreement with values obtained by Blecha & Štemprok (2012) from borehole data near Krásno village. The plotted pore throat size with respect to total porosity (Fig. 8d) of all measured samples suggests linear relation of the pore throat size and the total porosity of the whole dataset. However it doesn't show clustering on the relation path or markedly different course of linear relation for the individual granite types. It could suggest that the porosity is developed in all samples by similar mechanism, which is likely to be microfracturation as documented by microstructural observation of abundant microcracks (supplementary Fig. S1).

Both alteration processes led in studied granites to distinct changes in pore space volume and character. The process of feldspathization in the studied samples (20I and 15A) led to the decrease in free/total porosity ratio (13 and 14 %) and porosity in sample 15A (0.7 %). This can be explained by filling or discontinuation of pre-existing interconnected pores easily accessible for migrating low temperature hydrothermal fluids by growing of new generation of feldspars of small grain size. The metasomatic growth of new small crystals could produce closed pores not accessible for mercury (Geraud et al., 1993) and the microfracturation of the rock compensating microstructural changes is controlled by small grain size of the matrix, producing narrow and short microcracks (supplementary Fig. S1). The contradictory porosity characteristics observed in the sample 20VII are rather caused by microfracturing postdating the feldspathization, as the increase in total and free porosity is associated with increase in rock volume, which is unlikely at the lithostatic conditions and the sampling site as well as collected sample are lacking evidence for hydraulic fracturing during hydrothermal transformation.

Samples of greisenized leucogranites exhibit increase in total porosity (1.4 and 4.6 %), proportion of free porosity (27 and 38 %), pore size (0.34 and 0.7 μm) as well as skeletal density (2.66 and 2.76 gcm-3) alongside with maintained bulk density i.e. volume. The relatively high porosity and skeletal density of greisenized samples corresponds to values obtained by Štemprok et al. (1997). Nevertheless, the other pore space characteristics acquired by mercury injection porosimetry allow further interpretation of porosity development during the alteration processes. The main manifestation of greisenization process is metasomatic growth of Li-mica in microstructural point of view and influx of elements of higher atomic weight in geochemical perspective. The metasomatic replacement of less dense phases by high amount of denser Li-mica led during greisenization to the density increase of the granite. The density increase of the small part of the rock mass induces, at lithostatic conditions, development of local stress disequilibrium (i.e. tendency to decrease in volume). The easiest mechanism to accommodate such disequilibrium in brittle crust is fracturing of the rock mass. The growth of Li-mica also develops new flat planes of weakness on mica grain boundaries and cleavage planes feasible to accommodate mentioned stress disequilibrium. Development of such microcracks would produce net of interconnected and free porosity of relatively large size documented by mercury-injection measurements and observed abundant open microcracks on grain boundaries of newly formed Li-mica (supplementary Fig. S1). Such change in rock microstructure and porosity characteristics closely related to the mass transfer during metasomatic alteration differ from microstructural and porosity changes induced by granite alteration by weathering producing pores of small pore throat and characterized by low proportion of free porosity (Geraud et al., 1993).

7.4 Alteration processes as complex change of granite system

Flow of hydrothermal fluids through the rock matrix of granite alters substantially not only chemical composition, but also microstructure and physical properties through the metasomatic mineral changes. All these processes (chemical, microstructural and physical) are mutually connected.

The alkali feldspathization originated through fluid flow results in leaching of some mafic cations, decomposition of Li-mica and growth of new alkali feldspars. This causes decrease in magnetic susceptibility together with disruption of pore space by its discontinuation and infilling. However, the change of microstructure is not that important to modify, or even disrupt, the orientation of paramagnetic and diamagnetic phases aligned during granitic magma emplacement and thus does not significantly influence the AMS orientation.

In comparison, the greisenization has considerably larger effect on microstructure and physical properties of granite. Influx of elements of higher atomic weight with hydrothermal fluids induces growth of large amount of new phases (lithium mica, quartz, topaz and K-feldspar). This substantially alters the granite microstructure and mineral density of the rock matrix. The mineral density and microstructural change during the greisenization increase the porosity and size and character of pores to larger, flatter and probably more connected ones. The change of microstructure also leads to complete reworking of the original AMS and probably to decomposition of originally present fine-grained ferrimagnetic phase.

Acknowledgements

We greatly appreciate the constructive reviews by Y. Geraud and one anonymous colleague, as well as careful editorial handling by A. Kontny. This research was supported financially by the Czech National Foundation (GAČR) (grant no. 205/09/0540), by FCT (Fundação para a Ciência e a Tecnologia, Portugal) AMSProgress (PTDC/CTE-GIX/098696/2008) project, Czech Ministry of Education, Youth and Sports project LK 11202 (ROPAKO) and from institutional support to the Institute of Geophysics, Academy of Sciences of the Czech Republic (RVO 67985530). Matěj Machek is also grateful to SomaFM.

References

- *Ague J.J., 1994. Mass transfer during barrovian metamorphism of pelites, south-central connecticut; i, evidence for changes in composition and volume. Amer. J. Sci., 294, 989-1057.*

- *Alderton D.H.M., Pearce J.A. and Potts P.J., 1980. Rare earth element mobility during granite alteration: evidence from southwest england. Earth Planet. Sci. Lett., 49, 149-165.*

- *Beus A.A., 1962. Wall rock alterations of hydrothermal–pneumatolytic deposits of rare elements. Inter. Geol. Rev., 4, 1144-1153.*
- *Blecha V. and Štemprok M., 2012. Petrophysical and geochemical characteristics of late variscan granites in the Karlovy Vary massif (Czech republic) – implications for gravity and magnetic interpretation in shallow depths. J. Geosci., 57, 65-85.*
- *Bonin B., 2008. Death of super-continents and birth of oceans heralded by discrete A-type granite igneous events: the case of the Variscan–Alpine Europe. J. Geosci., 53, 237-252.*
- *Borradaile G. J., Jackson M., 2010. Structural geology, petrofabrics and magnetic fabrics (AMS, AARM, AIRM). J. Struct. Geol., 32, 1519-1551*
- *Bouchez J. L., 2000. Anistropie de susceptibilité magnétique et fabrique des granites, C. R. Acad. Sci., 330, 1-14. Boynton W.V., 1984. Cosmochemistry of the rare earth elements: meteorite studies. In: P. Henderson (Ed.), Rare Earth Element Geochemistry, Elsevier, Amsterdam, 63-114.*
- *Breiter K., Förster H.-J. and Seltmann R., 1999. Variscan silicic magmatism and related tin-tungsten mineralization in the erzgebirge–slavkovský les metallogenic province. Miner. Depos., 34, 505-521.*
- *Brown M., 2001. Crustal melting and granite magmatism: key issues. Phys. Chem. Earth (A), 26, 201-212.*
- *Bucholz C.E. and Ague J.J., 2010. Fluid flow and Al transport during quartz–kyanite vein formation, Unst, Shetland Islands, Scotland. J. Metamorph. Geol., 28, 19-39.*
- *Cathelineau M., 1986. Alkali metasomatism and quartz dissolution ('feldspathization´). J. Petrol., 27, 945-965.*
- *Chadima M., Jelínek V., 2008. Anisoft 4.2. – Anisotropy Data Browser. Paleo, Rock And Environmental Magnetism 11th Castle Meeting. Contributions to Geophysics and Geodesy, 38, 41.*
- *Chappell B.W., 2004. Towards a unified model for granite genesis. Trans. Roy. Soc. Edinb, Earth Sci., 95, 1-10. Clarke D.B., 1992. Granitoid Rocks, Chapman & Hall, London.*
- *Clemens J.D., 2003. S-type granitic magmas – petrogenetic issues, models and evidence. Earth Sci. Rev., 61, 1-18.*
- *Clemens J.D. and Droop G.T.R., 1998. Fluids, p–t paths and the fates of anatectic melts in the earth's crust. Lithos, 44, 21-36.*
- *Day R., Fuller M.D., Schmidt V.A., 1977. Hysteresis properties of titanomagnetites: grain size and composition dependence. Phys. Earth Planet. Int., 13, 260–266.*
- *De La Roche H., Leterrier J., Grandclaude P. and Marchal M., 1980. A classification of volcanic and plutonic rocks using r1r2-diagram and major element analyses – its relationships with current nomenclature. Chem. Geol., 29, 183-210.*
- *Debon F. and Le Fort P., 1983. A chemical–mineralogical classification of common plutonic rocks and associations. Trans. Roy. Soc. Edinb, Earth Sci., 73, 135-149.*
- *Dolejš D., Štemprok M., 2001. Magmatic and hydrothermal evolution of Li-F granites: Cínovec and Krásno intrusions, Krušné hory Batholith, Czech Republic. Bull. Czech Geol. Surv., 76, 77-99.*
- *Dolejš D., Wagner T., 2008. Thermodynamic modeling of non-ideal mineral-fluid equilibria in the system Si–Al–Fe–Mg–Ca–Na–K–H–O–Cl at elevated temperatures and pressures: Implications for hydrothermal mass transfer in granitic rocks. Geochim. Cosmochim. Acta, 72, 526-553.*

- *Dolníček Z., René M., Prochaska W. and Kovář M., 2012. Fluid evolution of the Hub stock, Horní Slavkov–Krásno Sn–W ore district, Bohemian Massif, Czech Republic. Miner. Depos., 47, 821-833.*
- *Dunlop D.J., 2002. Theory and application of the Day plot (M-rs/M-s versus H-cr/H-c) 1. Theoretical curves and tests using titanomagnetite data. J. Geophys. Res.-Solid Earth, 107, B3, 2056,*
- *Finger F., Gerdes A., René M., Riegler G., 2009. The SaxoDanubian Granite Belt: magmatic response to post-collisional delamination of mantle lithosphere below the south-western sector of the Bohemian Massif (Variscan orogen). Geol. Carpath., 60, 205-212.*
- *Förster H.-J., Romer R. L., 2010. Carboniferous magmatism. In: Linnemann U., Romer R. L. (eds.) Pre-Mesozoic Geology of Saxo-Thuringia – From the Cadomian Active Margin to the Variscan Orogen. Schweizerbart, Stuttgart, pp. 287-308.*
- *Förster H.-J., Tischendorf G., Seltmann R., Gotesmann B., 1998. Die variszischen Granite des Erzgebirges: neue Aspekte aus stofflicher Sicht. Z. geol. Wiss., 26, 31-60.*
- *Förster H.-J., Tischendorf G., Trumbull R. B., Gottesmann B., 1999. Late-collisional granites in the Variscan Erzgebirge (Germany). J. Petrol., 40, 1613-1645.*
- *Géraud Y., Mazerolle F. et Raynaud S. (1993).- Essai de quantification de la porosité d'un granite altéré. Utilisation du scanner médical (tomodensitométrie x). S.G.F, Bull. Soc. géol. France,164, 2, 243-253.*
- *Giesche H., 2006. Mercury porosimetry: A general (practical) overview. Part. Part. Syst. Charact., 23, 9–19.*
- *Grant J.A., 1986. The isocon diagram – a simple solution to Gresens' equation for metasomatic alteration. Econ. Geol., 81, 1976-1982.*
- *Grant J.A., 2005. Isocon analysis: A brief review of the method and applications. Phys. Chem. Earth (A), 30, 997-1004.*
- *Heinrich, C., 1990, The chemistry of hydrothermal tin(-tungsten) ore deposition. Econ. Geol. 85, 457-481.*
- *Hrouda, F. (1994) A technique for the measurement of thermal-changes of magnetic-susceptibility of weakly magnetic rocks by the Cs-2 apparatus and Kly-2 kappabridge. Geophys. Jour. Int., 118, pp. 604-612.*
- *Hrouda, F., 2004. Problems in interpreting AMS parameters in diamagnetic rocks. In: Martin-Hernandez F., Luneburg C., Aubourg C., Jackson M. (Ed.), Magnetic Fabric: Methods and Applications, Geo. Soc. Spec. Pub., 238, London, 49-59.*
- *Hrouda, F., Jelínek, V. and Hrušková, L. (1990) A package of programs for statistical evaluation of magnetic data using IBM-PC computers. AGU 1990 fall meeting. Eos, Transactions, American Geophysical Union, 71, pp. 1289.*
- *IAEA, 2011. Geological disposal facilities for radioactive waste, specific safety guide. IAEA Safety Standards Series No. SSG-14, International Atomic Energy Agency, Vienna.*
- *Irber W., 1999. The lanthanide tetrad effect and its correlation with K/Rb, Eu/Eu*, Sr/Eu, Y/Ho, and Zr/Hf of evolving peraluminous granite suites. Geochim. Cosmochim. Acta, 63, 489-508.*
- *Janoušek V., Farrow C. M., Erban V., 2006. Interpretation of whole-rock geochemical data in igneous geochemistry: Introducing geochemical data toolkit (GCDkit). J. Petrol., 47, 1255–1259.*

- *Janoušek V., Farrow C.M., Erban V. and Trubač J., 2011. Brand new Geochemical Data Toolkit (GCDkit 3.0) – Is it worth upgrading and browsing documentation? (Yes!). Geol. výzk. Mor. Slez., 18, 26-30.*
- *Jarchovský T., 2006. The nature and genesis of greisen stocks at Krásno, Slavkovský Les area – Western Bohemia, Czech Republic. J. Czech Geol. Soc., 51, 201-216.*
- *Jelínek, V. (1978) Statistical processing of anisotropy of magnetic susceptibility measured on groups of specimens. Stud. Geophys. Geod., 22, 50-62.*
- *Jelínek, V. and Pokorný, J. (1997) Some new concepts in technology of transformer bridges for measuring susceptibility anisotropy of rocks. Phys. Chem. Earth, 22, 179-181.*
- *Just J. and Kontny A., 2012. Thermally induced alterations of minerals during measurements of the temperature dependence of magnetic susceptibility: a case study from the hydrothermally altered Soultz-sous-Forêts granite, France. Int. J. Earth. Sci., 101, 819–839.*
- *Kempe U., Bombach K., Schlothauer T., Hutschenreuter J., Wolf D., Matukov D. and Sergeev S., 2004. Pb/Pb and U/Pb zircon dating of subvolcanic rhyolite as a time marker for hercynian granite magmatism and Sn mineralisation in the Eibenstock granite, Erzgebirge, Germany: Considering effects of zircon alteration. Miner. Depos., 39, 646-669.*
- *Keppler H. and Wyllie P.J., 1990. Role of fluids in transport and fractionation of uranium and thorium in magmatic processes. Nature, 348, 531-533.*
- *Kovaříková P., Siebel W., Jelínek E., Štemprok M., Kachlík V., Holub F.V. and Blecha V., 2007. Petrology, geochemistry and zircon age for redwitzite at Abertamy, NW Bohemian Massif (Czech Republic): Tracing the mantle component in late variscan intrusions. Chem. Erde, 67, 151-174.*
- *Kovaříková P., Siebel W., Jelínek E., Štemprok M., Kachlík V., Holub F.V. and Blecha V., 2010. Dioritic intrusions of the Slavkovský Les (Kaiserwald), Western Bohemia: Their origin and significance in late variscan granitoid magmatism. Int. J. Earth Sci., 99, 545-565.*
- *Li Y. and Wardlaw N. C. 1986a. The influence of wettability and critical pore-throat size ratio on snap-off. J. Colloid Interface Sci., 109, 461–472.*
- *Li Y. and Wardlaw N. C. 1986b. Mechanism of non wetting phase trapping during imbibition at slow rates. J. Colloid Interface Sci., 109, 473–486.*
- *Machek M., Kratinová Z., René. M., Janoušek V., Roxerová Ž., (2011) Nature and petrogenesis of topaz-bearing granites – a case study of the Krudum granite body (Slavkovský les Mts., Czech Republic). 9th CETEG Meeting. Trav. Geophys., XL, 78.*
- *Masuda A., Kawakami O., Dohmoto Y. and Takenaka T., 1987. lanthanide tetrad effects in nature: Two mutually opposite types, W and M. Geochem. J., 119-124.*
- *Monecke T., Kempe U., Monecke J., Sala M. and Wolf D., 2002. tetrad effect in rare earth element distribution patterns; a method of quantification with application to rock and mineral samples from granite-related rare metal deposits. Geochim. Cosmochim. Acta, 66, 1185-1196.*
- *Monecke T., Kempe U., Trinkler M., Thomas R., Dulski P. and Wagner T., 2011. Unusual rare earth element fractionation in a tin-bearing magmatic–hydrothermal system. Geology, 39, 295-298*
- *Nabelek P.I. and Liu M., 2004. Petrologic and thermal constraints on the origin of leucogranites in collisional orogens. Trans. Roy. Soc. Edinb, Earth Sci., 95, 73-85.*

- *Nur A. and Simmons G., 1969. The effect of saturation on velocity in low porosity rocks. Earth Planet. Sci. Lett., 7, 183–193.*
- *Paterson S. R., Fowler JrMcCaffrey K.J.W. and Vigneresse J.L., 2000. Granite magma formation, transport and emplacement in the Earth's crust. Nature, 408, 669-673.*
- *Pitcher W.S., 1993. The Nature and Origin of Granite, Chapman & Hall, London.*
- *Pollard P. J., 1983. Magmatic and postmagmatic processes in the formation of rocks associated with rare-element deposits. Trans. Inst. Min. Metal., B92, 1-9.*
- *René M., 1998. Development of topaz-bearing granites of the Krudum massif (Karlovy Vary pluton). Acta Univ. Carol. , Geol., 42, 103-109.*
- *René M. and Škoda R., 2011. Nb–Ta–Ti oxides fractionation in rare-metal granites: Krásno–Horní Slavkov ore district, Czech Republic. Mineral. Petrol., 103, 37-48.*
- *Rochette P., Aubourg C., and Perrin M., 1999. Is this magnetic fabric normal? A review and case studies in volcanic formations. Tectonophysics, 307, 219–234.*
- *Romer R.L., Thomas R., Stein H.J. and Rhede D., 2007. Dating multiply overprinted Sn-mineralized granites – Examples from the Erzgebirge, Germany. Miner. Depos., 42, 337-359.*
- *Rosener M. and Géraud Y., 2007. Using physical properties to understand the porosity network geometry evolution in gradually altered granites in damage zones. Geological Society, London, Special Publications; 284; 175-184.*
- *Rubin J.N., Henry C.D. and Price J.G., 1993. The mobility of zirconium and other 'immobile' elements during hydrothermal alteration. Chem. Geol., 110, 29-47.*
- *Sawyer E.W., Cesare B. and Brown M., 2011. When the continental crust melts. Elements, 7, 229-234.*
- *Scherba G. N., 1970. Greisens. Inter. Geol. Rev., 12, 114-150.*
- *Staněk M., Géraud Y., Lexa O., Špaček P., Ulrich S., Diraison M., 2013. Elastic anisotropy and pore space geometry of schlieren granite: direct 3-D measurements at high confining pressure combined with microfabric analysis. Geophys. J. Int., 194, 383-394.*
- *Štemprok, M., 1987. Greisenization (a review). Geol. Rundsch. 76, 169-175.*
- *Štemprok, M., Chlupáčová, M., Pivec, E., Novák, JK and Lang, M., 1997. Petrochemical and petrophysical changes caused by greisenization in the younger granites of the Krušné hory Batholith (Czech Republic). In: Papunen H. (Ed.), Mineral Deposits, Balkema, Rotterdam, 679–682.*
- *Surma F. and Geraud Y., 2003. Porosity and thermal conductivity of the Soultz-sous-Forêts granite. Pure And Applied Geophysics, 160, 1125-1136.*
- *Tarling D.H. and Hrouda F., 1993. The Magnetic Anisotropy of Rocks. Chapman and Hall, London, 232p.*
- *Veksler I.V., Dorfman A.M., Kamenetsky M., Dulski P. and Dingwell D.B., 2005. Partitioning of lanthanides and Y between immiscible silicate and fluoride melts, fluorite and cryolite and the origin of the lanthanide tetrad effect in igneous rocks. Geochim. Cosmochim. Acta, 69, 2847-2860.*
- *Vigneresse J.L., 2004. A new paradigm for granite generation. Trans. Roy. Soc. Edinb, Earth Sci., 95, 11-22.*

- *Villaseca C., Barbero L. and Herreros V., 1998. A re-examination of the typology of peraluminous granite types in intracontinental orogenic belts. Trans. Roy. Soc. Edinb, Earth Sci., 89, 113-119.*
- *Wardlaw N. C., Li Y. and Forbes D. 1987. Porethroat size correlation from capillary pressures curves. Transp. Porous Media, 2, 597–614.*
- *Washburn E. W. 1921. Note on a method of determining the distribution of pore sizes in a porous material. Proc. Natl. Acad. Sci. U. S. A., 7, 115–116.*
- *Webster J., Thomas R., Forster H., Seltmann R., Tappen, C. 2004. Geochemical evolution of halogen-enriched granite magmas and mineralizing fluids of the Zinnwald tin-tungsten mining district, Erzgebirge, Germany. Miner. Depos., 39, 452-472.*
- *Witt W.K., 1988. Evolution of high-temperature hydrothermal fluids associated with greisenization and feldspathic alteration of a tin-mineralized granite, Northeast Queensland. Econ. Geol., 83, 310-334.*
- *Zhao Z.H., Xiong X.L., Hen X.D., Wang Y.X., Qiang W., Bao Z.W. and Jahn B., 2002. Controls on the REE tetrad effect in granites: evidence from the Qianlishan and Baerzhe granites, China. Geochem. J., 36, 527-543. . T. K., Schmidt K. L., Yoshinobu A. S., Yuan E. S., Miller, R. B. 1998. Interpreting magmatic fabric patterns in plutons. Lithos, 44, 53–82.*
- *Paterson S.R., Vernon R.H., Tobisch, O.T. 1989. A review of criteria for the identification of magmatic and tectonic foliations in granitoids. J. Struct. Geol., 11, 349–363.*
- *Petford N., Cruden A.R., McCaffrey K.J.W. and Vigneresse J.L., 2000. Granite magma formation, transport and emplacement in the Earth's crust. Nature, 408, 669-673.*
- *Pitcher W.S., 1993. The Nature and Origin of Granite, Chapman & Hall, London.*
- *Pollard P. J., 1983. Magmatic and postmagmatic processes in the formation of rocks associated with rare-element deposits. Trans. Inst. Min. Metal., B92, 1-9.*
- *René M., 1998. Development of topaz-bearing granites of the Krudum massif (Karlovy Vary pluton). Acta Univ. Carol. , Geol., 42, 103-109.*
- *René M. and Škoda R., 2011. Nb–Ta–Ti oxides fractionation in rare-metal granites: Krásno–Horní Slavkov ore district, Czech Republic. Mineral. Petrol., 103, 37-48.*
- *Rochette P., Aubourg C., and Perrin M., 1999. Is this magnetic fabric normal? A review and case studies in volcanic formations. Tectonophysics, 307, 219–234.*
- *Romer R.L., Thomas R., Stein H.J. and Rhede D., 2007. Dating multiply overprinted Sn-mineralized granites – Examples from the Erzgebirge, Germany. Miner. Depos., 42, 337-359.*
- *Rosener M. and Géraud Y., 2007. Using physical properties to understand the porosity network geometry evolution in gradually altered granites in damage zones. Geological Society, London, Special Publications; 284; 175-184.*
- *Rubin J.N., Henry C.D. and Price J.G., 1993. The mobility of zirconium and other 'immobile' elements during hydrothermal alteration. Chem. Geol., 110, 29-47.*
- *Sawyer E.W., Cesare B. and Brown M., 2011. When the continental crust melts. Elements, 7, 229-234.*
- *Scherba G. N., 1970. Greisens. Inter. Geol. Rev., 12, 114-150.*
- *Staněk M., Géraud Y., Lexa O., Špaček P., Ulrich S., Diraison M., 2013. Elastic anisotropy and pore space geometry of schlieren granite: direct 3-D measurements at high confining pressure combined with microfabric analysis. Geophys. J. Int., 194, 383-394.*

- *Štemprok, M., 1987. Greisenization (a review). Geol. Rundsch. 76, 169-175.*
- *Štemprok, M., Chlupáčová, M., Pivec, E., Novák, JK and Lang, M., 1997. Petrochemical and petrophysical changes caused by greisenization in the younger granites of the Krušné hory Batholith (Czech Republic). In: Papunen H. (Ed.), Mineral Deposits, Balkema, Rotterdam, 679–682.*
- *Surma F. and Geraud Y., 2003. Porosity and thermal conductivity of the Soultz-sous-Forêts granite. Pure And Applied Geophysics, 160, 1125-1136.*
- *Tarling D.H. and Hrouda F., 1993. The Magnetic Anisotropy of Rocks. Chapman and Hall, London, 232p.*
- *Veksler I.V., Dorfman A.M., Kamenetsky M., Dulski P. and Dingwell D.B., 2005. Partitioning of lanthanides and Y between immiscible silicate and fluoride melts, fluorite and cryolite and the origin of the lanthanide tetrad effect in igneous rocks. Geochim. Cosmochim. Acta, 69, 2847-2860.*
- *Vigneresse J.L., 2004. A new paradigm for granite generation. Trans. Roy. Soc. Edinb, Earth Sci., 95, 11-22.*
- *Villaseca C., Barbero L. and Herreros V., 1998. A re-examination of the typology of peraluminous granite types in intracontinental orogenic belts. Trans. Roy. Soc. Edinb, Earth Sci., 89, 113-119.*
- *Wardlaw N. C., Li Y. and Forbes D. 1987. Porethroat size correlation from capillary pressures curves. Transp. Porous Media, 2, 597–614.*
- *Washburn E. W. 1921. Note on a method of determining the distribution of pore sizes in a porous material. Proc. Natl. Acad. Sci. U. S. A., 7, 115–116.*
- *Webster J., Thomas R., Forster H., Seltmann R., Tappen, C. 2004. Geochemical evolution of halogen-enriched granite magmas and mineralizing fluids of the Zinnwald tin-tungsten mining district, Erzgebirge, Germany. Miner. Depos., 39, 452-472.*
- *Witt W.K., 1988. Evolution of high-temperature hydrothermal fluids associated with greisenization and feldspathic alteration of a tin-mineralized granite, Northeast Queensland. Econ. Geol., 83, 310-334.*
- *Zhao Z.H., Xiong X.L., Hen X.D., Wang Y.X., Qiang W., Bao Z.W. and Jahn B., 2002. Controls on the REE tetrad effect in granites: evidence from the Qianlishan and Baerzhe granites, China. Geochem. J., 36, 527-543.*

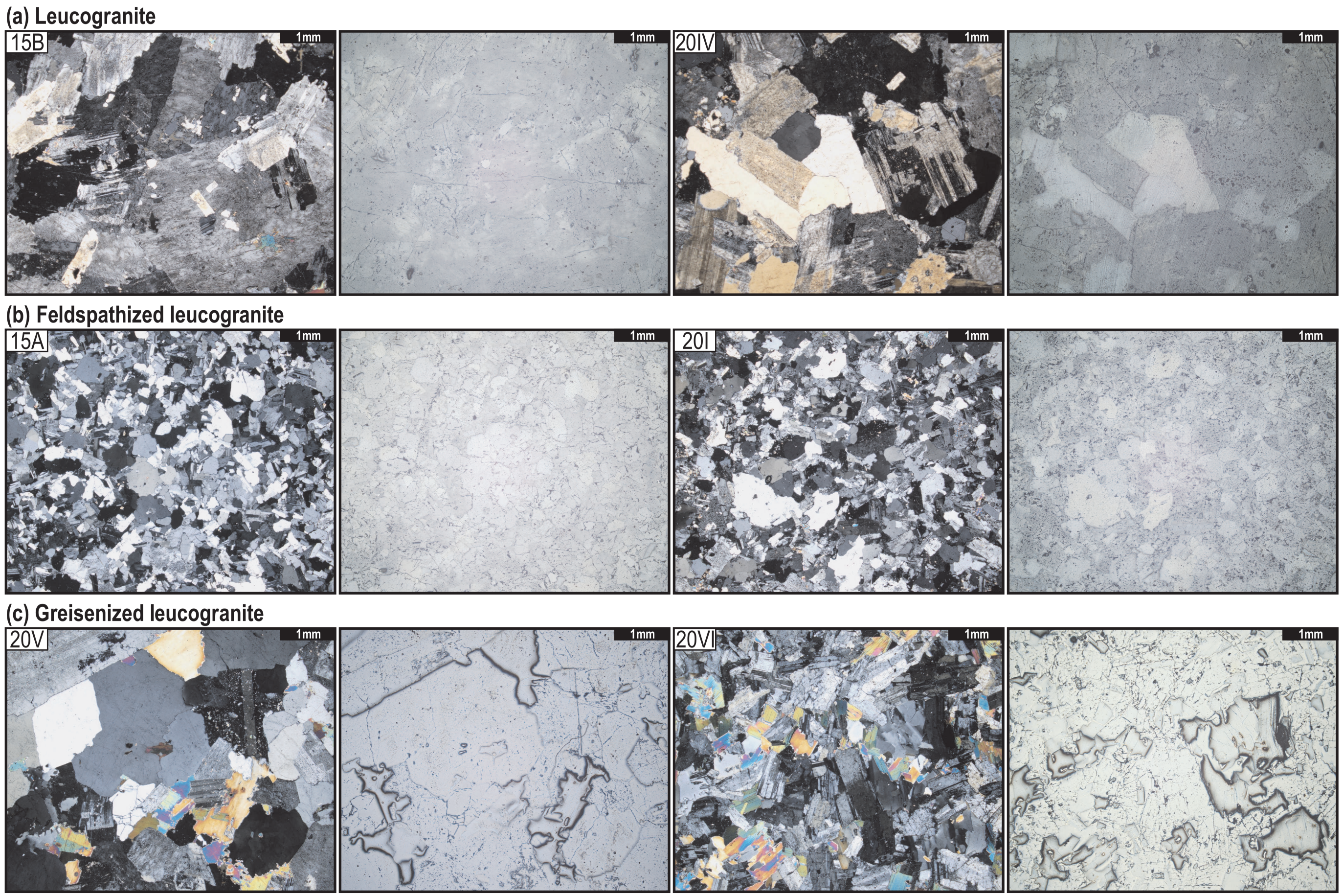

Fig. S1 *Microphotographs of selected samples representing individual granite types in cross-polarized and reflected light.*